NISTIR 6183

Preparation and Characterization of Polymer/Dendrimer Blends Progress Report 2/24/97

Eric J. Amis
Barry J. Bauer
Andreas Topp
Ty J. Prosa
Dawei Liu
Catheryn L. Jackson
Alamgir Karim
Jack Douglas

U.S. DEPARTMENT OF COMMERCE
Technology Administration
National Institute of Standards
and Technology
Polymers Division
Bldg. 220, Room B124
Gaithersburg, MD 20899-0001

NIST

NISTIR 6183

Preparation and Characterization of Polymer/Dendrimer Blends Progress Report 2/24/97

Eric J. Amis
Barry J. Bauer
Andreas Topp
Ty J. Prosa
Dawei Liu
Catheryn L. Jackson
Alamgir Karim
Jack Douglas

U.S. DEPARTMENT OF COMMERCE
Technology Administration
National Institute of Standards
and Technology
Polymers Division
Bldg. 220, Room B124
Gaithersburg, MD 20899-0001

June 1998

U.S. DEPARTMENT OF COMMERCE
William M. Daley, Secretary

TECHNOLOGY ADMINISTRATION
Gary R. Bachula, Acting Under Secretary
for Technology

NATIONAL INSTITUTE OF STANDARDS
AND TECHNOLOGY
Raymond G. Kammer, Director

Table of Contents

General Information

Throughout this report certain conventions will be used when describing uncertainties in measurements. Plots of small angle scattering data have been calculated from circular averaging of two dimensional files. The uncertainties are calculated as the estimated standard deviation of the mean and the total combined uncertainty is not given as comparisons are made with data obtained under the same conditions. In cases where the limits are smaller then the plotted symbols, the limits are left out for clarity. In data plots with uncertainties larger than the symbols, representative confidence limits are plotted at appropriate places. Fits of the scattering data are made by a least squares fit of the data giving an average and a standard deviation to the fit, this is true for fit values such as radius of gyration and exponents. Temperatures are given as expected ranges of values based on previous work.

All concentrations are calculated from weighed samples and are reported as mass fractions and are nominal values for naming purposes. The range of the concentrations calculated from weight are within one percent of the reported value. The conventional notation "molecular weight" has been replaced by "relative molecular mass" in most cases. Rarely, the conventional notation is used to conform to previous publications.

Certain commercial materials and equipment are identified in this paper in order to specify adequately the experimental procedure. In no case does such identification imply recommendation by the National Institute of Standards and Technology nor does it imply that the material or equipment identified is necessarily the best available for this purpose.

This work is supported in part by the U.S. Army Research Office under contract number 35109-CH.

DSC of Dendrimer, Dendrigraft and Hyperbranched Blends

NIST: Dawei Liu, Barry J. Bauer, Eric J. Amis

Outside Collaborators: Donald Tomalia, MMI; Rui Yin, MMI; Rolf Scherrenberg, DSM

Objectives:

To use thermal methods to determine the miscibility of blends of dendrimers, dendrigrafts, or hyperbranched with linear polymers.

Technical Description:

Differential scanning calorimetry (DSC) was used to measure glass transition temperatures (T_g) of blends of dendritic and linear polymers to look for shifted, single transitions.

Summary Report:

The miscibility of blends can be quickly screened by visual observations and DSC of cast films. For miscibility to be present, the blends must be optically clear and have a T_g intermediate between those of the blend components. The advantages are that contrast (neutron or x-ray) is not necessary and molecular mass or size is not important. Limitations of this technique include:

1. A solvent effect in which phase separation occurs during the drying process even for a miscible blend.
2. Refractive indices of the polymers being too close together to look cloudy when phase separated.
3. T_g's that are too close together or too weak to be seen.
4. Blends made from compositions near 0 % or 100 % can make phase separation difficult to determine.

Four types of branched polymers were studied, polyamidoamine (PAMAM) dendrimers (both full and half generations), DSM diaminobutane dendrimers, poly(ethyl oxazoline) (PEOX) dendrigraft and hyperbranched, and polyol hyperbranched. Two classes of linear polymers were used, commercial polymers and custom synthesized deuterated polymers for neutron scattering. Most of the linear polymers contain groups capable of strong interactions such as hydrogen bonding or ionic interactions.

Table 1 lists the polymer combinations tested along with the optical clarity observations and measured T_g's. The range of T_g's is typically ± 3 °C as determined by replicate measurements, and compositions listed are nominal values. In many cases the cast films were cloudy and DSC measurements were not taken. The custom synthesized samples

are identified by lab book codes and are identified at the end of the table. The PAMAM dendrimers were miscible with either poly(methyl methacrylate) (PMMA)-d8 or polystyrene (PS)-d8 if the correct amount of methacrylic acid (MAA) comonomer was used giving -COOH groups that could interact with the amino groups. PS with hexafluoroisopropyl groups was not miscible with the PAMAM dendrimers tested. The DSM dendrimers and hyperbranched polyols had apparent miscibility with some polymers having natural hydrogen bonding capability.

Many of the blends that had optical clarity and a single T_g had unusual DSC curves at higher temperatures. It is likely that chemical reactions are taking place, placing covalent bonds between the blended polymers. This will lead to a single phase and molecularly dispersed dendrimers, but it is not a blend in the conventional sense (see description in accompanying report on SANS of blends). Also included in this table are interpenetrating polymer networks (IPN) made with G4 PAMAM and 2-hydroxyethyl methacrylate (HEMA).

PEOX is known to be miscible with poly(styrene-co-acrylonitrile) (PSAN) that has about 25 % acrylonitrile. PEOX dendrigrafts were blended with a deuterated PSAN and characterized by DSC and SANS. Blends appeared to be miscible for all types of PEOX studied, linear, hyperbranched, and generations G0 - G2 dendrigrafts. Figure 1 compares the T_g's of pure components and 50 % blends. The blend T_g's are between those of the components, and there might be slight variations depending on PEOX type. Figure 2 is a plot of T_g of hyperbranched PEOX/PSAN blends versus composition. The T_g's continuously change between the limits. For additional information see accompanying report on SANS of PEOX solutions and blends.

Future Plans:

These screening techniques will be used to screen a wide variety of commercial and custom made polymers. The most promising cases found with the largest dendrimers (G7 - G10 PAMAM) will be examined by TEM. Miscible blends will be examined by SAXS using natural contrast, and by SANS using deuteration.

TYPE	GENER	LINEAR POLY	CLARITY	T_g
PAMAM	G4	BI6(10%)*	CLEAR	62
		BI6(20%)	CLEAR	63
		BI6(30%)	CLEAR	64
		BI7(30%)	CLOUDY	-6,53
		CC1(30%)**	CLEAR	58
		CC2(30%)	CLEAR	66
		CC3(30%)	WHITE	--
		BW1(30%)+	WHITE	--
		BW2(30%)	WHITE	--
		PVME-99000	CLEAR	0
		PVME-30000	CLEAR	7
		PVP	CLEAR	-4
		HEMA/MAA(5%)	CLEAR	71
		HEMA/MAA(10%)	CLEAR	73
		HEMA/MAA(20%)	CLEAR	70
		HEMA(5%)	CLEAR	75
		HEMA(10%)	CLEAR	51
		HEMA(20%)	CLEAR	13
		PHEA	CLEAR	--
	G3.5	PVME-99000	CLEAR	18
		PVME-30000	CLOUDY	--
		PVP	CLEAR	22,82
		PHEA	CLEAR	2
		BI7*	CLOUDY	--
		PEI(10%)	WHITE	--
		PEI(30%)	WHITE	--
		PEI(50%)	WHITE	--
		PEI(70%)	WHITE	--
		PEI(90%)	WHITE	--
DSM	G3	PVA	CLEAR	30
		PHEA	CLEAR	-4
		PEG	CLEAR	8
		PEI (LOW)	CLEAR	-21
		PEI(HIGH)	CLOUDY	-9
POLYOL	G5	PHEA	CLEAR	20
		PEG	CLEAR	-10
		PEI(LOW)	CLEAR	15
		PEI(HIGH)	CLOUDY	27
PEOX	100_3-50	CQ1(50%)++	CLEAR	83
	100_2-50	CQ1(50%)	CLEAR	76
	100_1-50	CQ1(50%)	CLEAR	78

HPB 500-20	CQ1(10%)	CLEAR	62
	CQ1(30%)	CLEAR	62
	CQ1(50%)	CLEAR	77
	CQ1(70%)	CLEAR	79
	CQ1(90%)	CLEAR	98
200	CQ1(50%)	CLEAR	72

Table 1. Optical clarity and DSC results of dendrimer, dendrigraft, and hyperbranched blends.

NOTES:

BI* : Methylmathacrylate-d8 + Methacrylic Acid

BI6: 2% MAA + 98% PMMA
BI7: 100% PMMA

CC**: Styrene-d8 + Methacrylic Acid

CC1: 0.8% MAA + 99.2% PS
CC2: 2.4% MAA + 97.6% PS
CC3: 8.0% MAA + 92.0% PS

BW+ : Styrene-d8 + 4-Hexafluoroisopyl-a-methylstyrene

BW1: 3% 4-Hexafluoro Isoprene Styrene + 97% PS
BW2: 10% 4-Hexafluoro Isoprene Styrene + 90% PS

CQ++: Styrene-d8 + Acrylonitrile

CQ1: 25% PSAN + 75% PS

PVME: Poly(vinylmethyl ether)

HEMA: 2-hydroxyethyl methacrylate

MAA: Methacrylic acid

PHEA: Poly(2-hydroxyethyl acrylate)

PVP: Poly(2-vinylpyridine)

PEG: Poly(ethylene glycol)

PEI: Poly(ethylene imine)

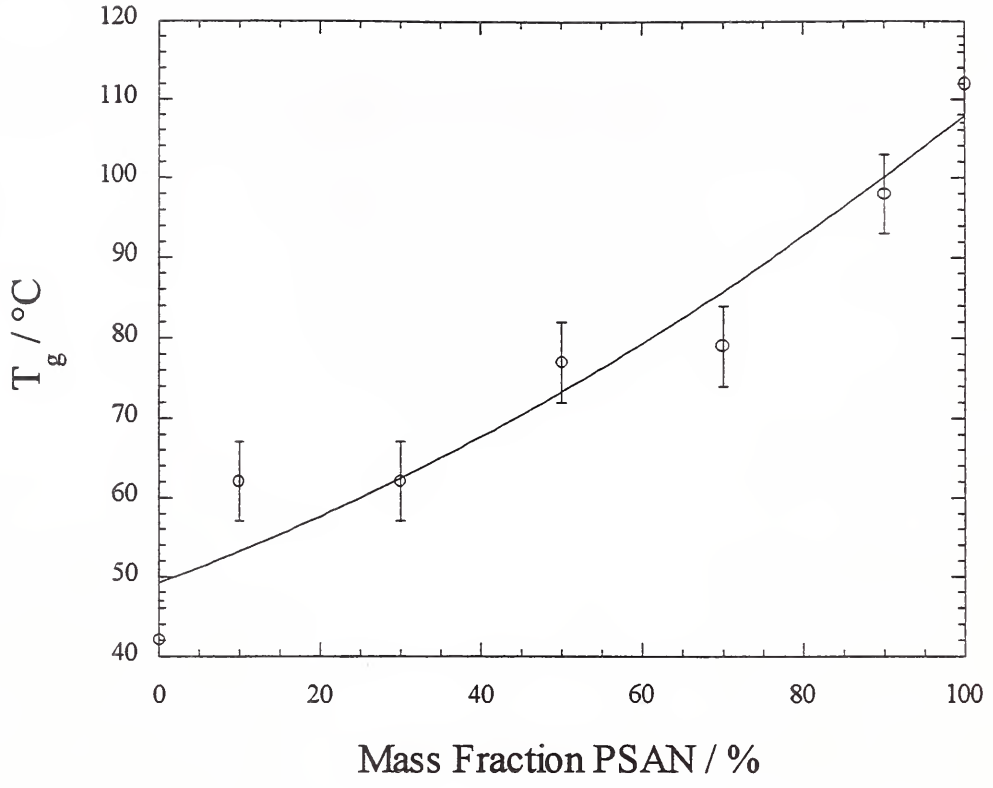

Figure 1. Glass transition temperature of PEOX HPB (500-20) / PSAN blend.

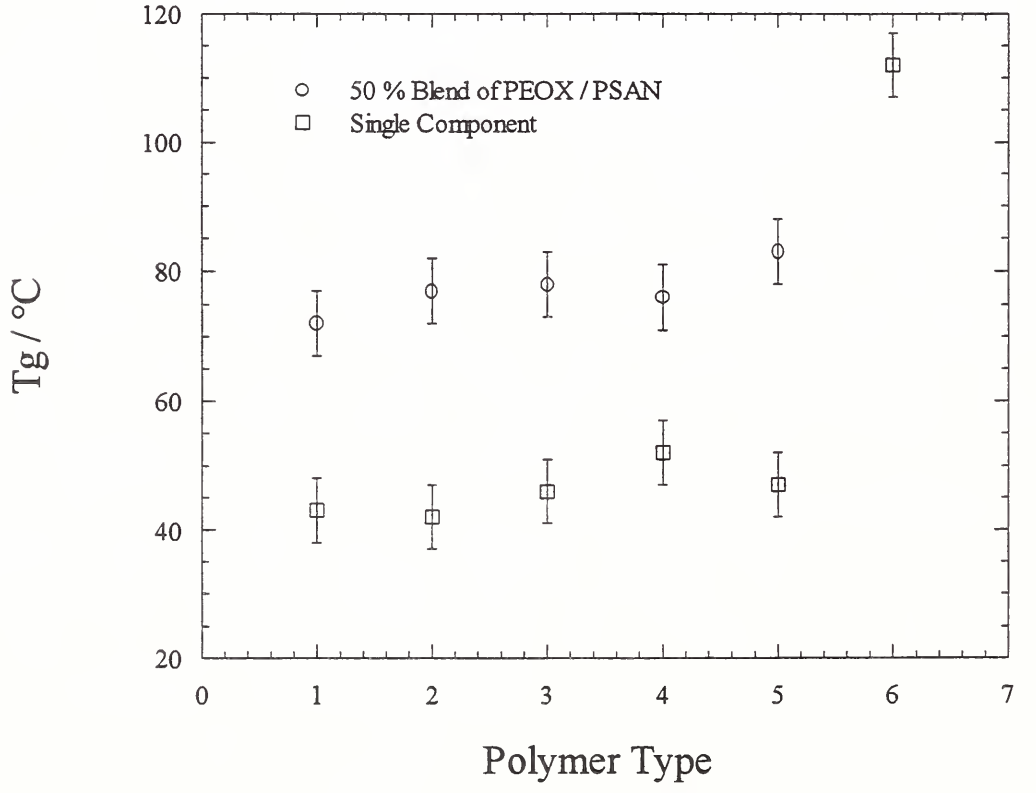

Figure 2. Glass transition temperatures of PEOX polymers and blends with 25% PSAN.

SANS and SAXS of Dendrimer Blends and IPNs

NIST: Andreas Topp, Ty J. Prosa, Dawei Liu, Barry J. Bauer, Eric J. Amis

Outside Collaborators: Donald Tomalia, MMI

Objectives:

To use small angle neutron scattering (SANS) and small angle x-ray scattering (SAXS) to determine the miscibility of blends of dendrimers, dendrigrafts, or hyperbranched with linear polymers or interpenetrating polymer networks (IPN).

Technical Description:

Interpenetrating polymer network (IPN) and blending techniques are used to synthesize samples of dendritic and linear polymers. They are characterized by small angle scattering techniques which determine if the dendritic polymers are molecularly dispersed.

Summary Report:

Single phase combinations of PAMAM dendrimers and conventional polymers were studied by small angle scattering techniques. SANS required contrast to be enhanced by deuteration of the linear component. SAXS relied on natural contrast of the components, and sometimes the contrast was enhanced by swelling with solvents having different electron densities. Many additional combinations that did not have sufficient scattering contrast were studied by other techniques (such as optical clarity and DSC) are discussed elsewhere.

The SANS experiments used styrene-d8 or methyl methacrylate-d8 as the primary component of the linear polymer. To induce a specific interaction between the linear polymer and the dendrimer, between (1 and 10) % of either methacrylic acid (ionic interaction) or p-hexafluoroisopropyl alpha methyl styrene (hydrogen bonding) was copolymerized with the deuterated monomer. All of the samples were solvent cast and screened for clarity by visual observation and for blend T_g by DSC. Out of all of the combinations, random copolymers of PMMA-d8 and PMAA proved most promising, giving clear films with intermediate T_g's.

Figure 3 shows the scattering from a blend of 50 % G11 PAMAM dendrimer with PMMA-r-PMAA containing 2 % PMAA. The scattering is typical of a single phase mixture. The scattering decreased with increasing the temperature from 140 °C to 180 °C, indicating decreased concentration fluctuations due to enhanced mixing. Figure 4 shows DSC results from this combination, with the blend having a T_g intermediate between the pure materials. At higher temperatures, the blend showed an anomalous change in the heat flow. This is often found in systems that are undergoing chemical reactions.

Figure 5 gives the SANS results of a G4 dendrimer and the same polymethacrylate going from 130 °C up to 180 °C and back to 130 °C. The scattering is not reproducible, decreasing in intensity continuously. This is likely to be a chemical reaction between the dendrimer and the methacrylate polymer. After the SANS experiment, the samples were no longer soluble, indicating that crosslinking took place.

An attempt was made to use SAXS to examine the blends used in SANS but the natural contrast was not sufficient to produce significant scattering. IPNs were synthesized with (5, 10 or 20) % of G4 dendrimer in 2- hydroxyethyl methacrylate. Three samples were also made with an addition of a stoichiometric amount of methacrylic acid to the terminal $-NH_2$ groups of the dendrimer. The acid addition was an attempt to induce the long range order that has been previously seen in solutions. SAXS of the as-polymerized IPNs did not show any structure, probably due to lack of contrast. To improve the contrast, methanol was added to the to preferentially swell one component. This allows the structure to be probed.

The swollen IPNs are three component systems, the PHEMA network, the dendrimer and the methanol. To extract structural information, the scattering from the acidified IPN is divided by the scattering from an unacidified network of the same dendrimer content. This ratio is most strongly dependent on the average spacing of the dendrimers in the acidified system compared to that of the unacidified, random system. Figure 6 is a plot of such ratios for the above system. At 5 %, no peak can be observed, but at (10 and 20) %, a peak emerges and moves to larger angle. This suggests that there is a prefered spacing between dendrimers that changes with concentration, as has been seen in dendrimer solutions.

Single phase combinations of dendrimers and other polymers have been identified, but chemical bonding between the components is also present. The primary amino terminal groups and interior amide linkages are prone to react chemically with other polymers. These can be studied by techniques such as SANS, SAXS, DSC, and TEM, to exhibit a molecular dispersion of dendrimers in a solid matrix.

Future Plans:

There is still a need to identify a miscible blend that does not chemically bond during the course of the experiment. To do this two approaches can be used. First, we will try to identify a miscible polymer that does not have chemistry that can react with PAMAM as is possible for polymers containing acid, ester, amide, hydroxy, or amine groups. Secondly, we will use a dendrimer that has different functional groups. The diaminobutane dendrimers are a candidate for this, along with polyether types that have been reported.

In miscible blends that form covalent bonds between the components, the miscibility and reactivity may give opportunity to examine the use as dendrimers as hyperfunctional crosslinking sites.

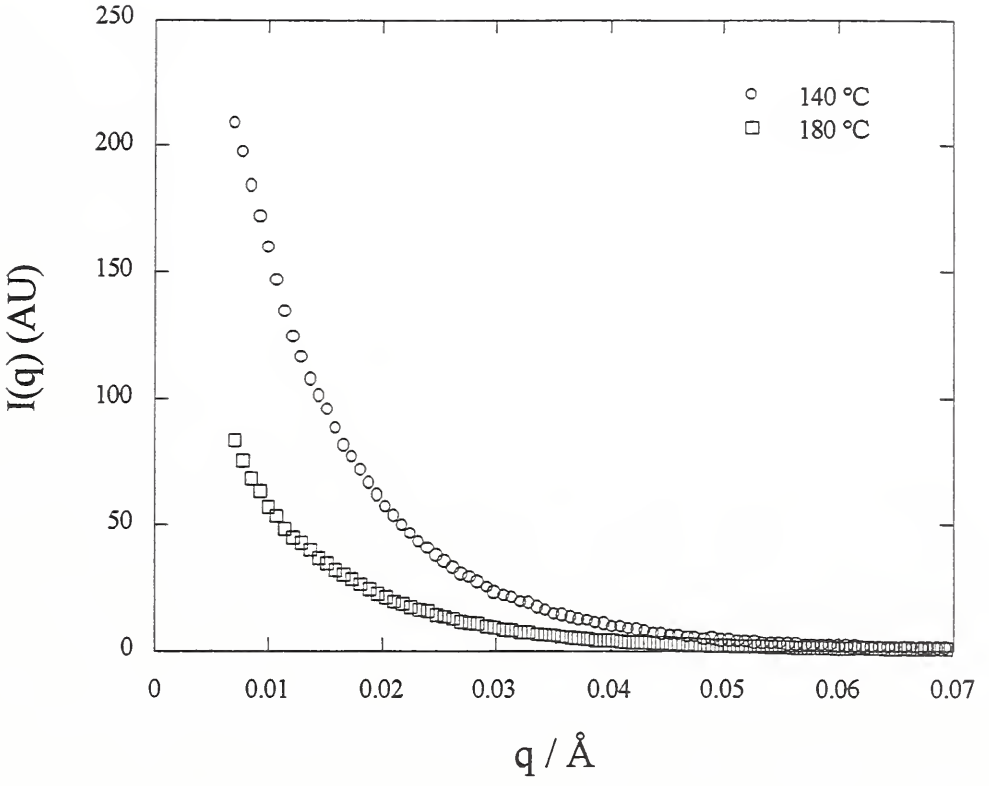

Figure 3. SANS of PMMA-r-PMAA/PAMAM G11 Blend.

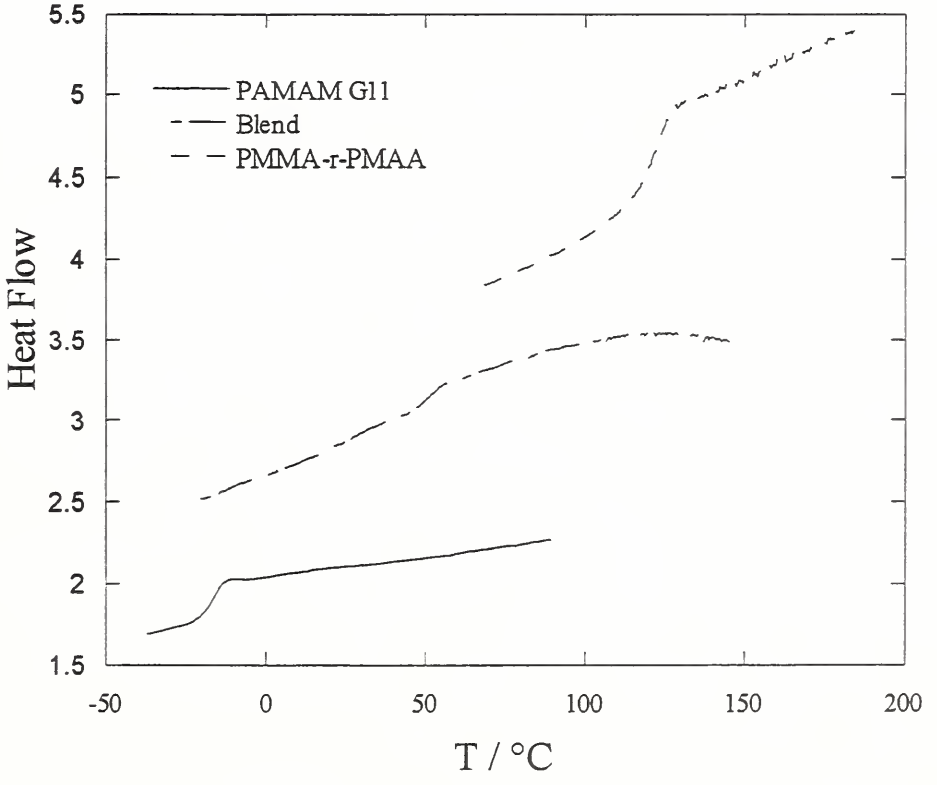

Figure 4. DSC of PMMA-r-PMAA. PAMAM G11, and a blend of the two.

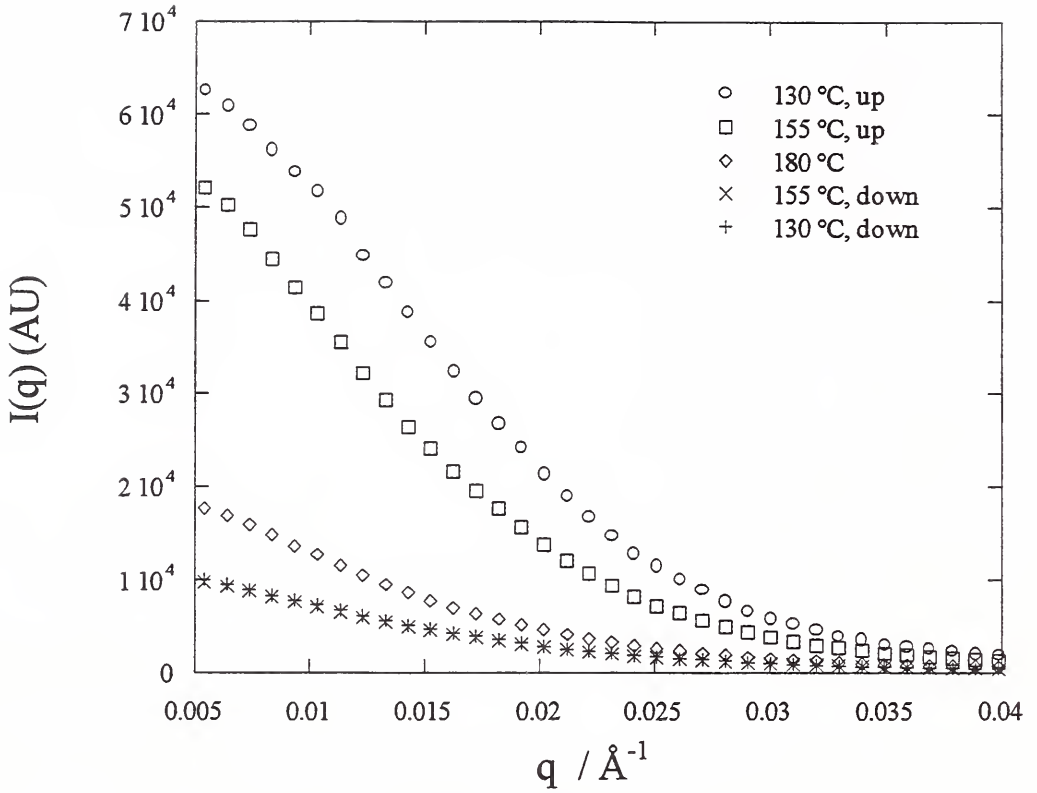

Figure 5. SANS of blend of PMMA-r-PMAA/PAMAM G4 cycled up and down in temperature.

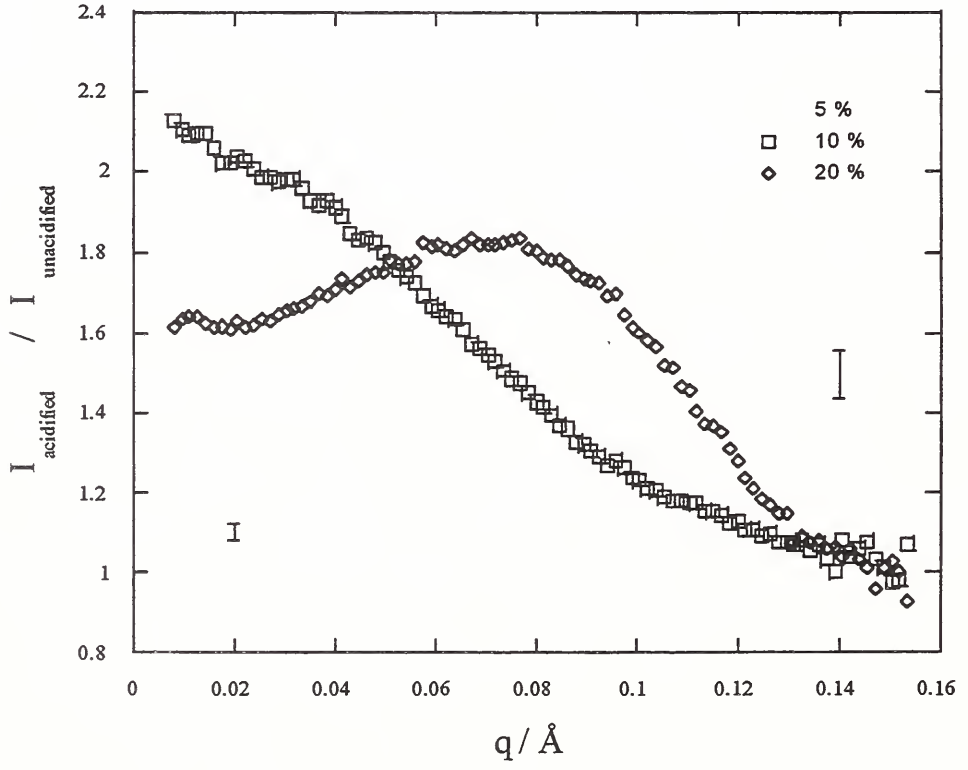

Figure 6. SAXS of IPNs of PHEA/PAMAM G4 swollen in methanol.

SANS of PEOX Solutions and Blends

NIST: Andreas Topp, Barry J. Bauer, Eric J. Amis

Outside Collaborators: Donald Tomalia, MMI; Rui Yin, MMI.

Objectives:

To use SANS to characterize dendrigraft polymers, measuring their molecular mass, radius of gyration, intermolecular interactions, and miscibility with other polymers.

Technical Description:

SANS is used on dilute solutions to determine single molecule characteristics and on concentrated solutions for intermolecular interactions. Deuterated polymers are synthesized for use in SANS to measure miscibility.

Summary Report:

The PEOX samples studied were linear PEOX with reported degrees of polymerization of 200 and 300, hyperbranched (500-20) and (500-100), and dendrigrafts ($100_{(G+1)}$-50) and ($100_{(G+1)}$-100) (generations 0-3). Dendrigrafts (100_4-50) and (100_3-100) did not fully dissolve in any solvent tried including acetone, methanol, methylene chloride, and DMF. These samples were not used in the SANS experiments.

Figure 7 is a plot of the molecular mass calculated from both Zimm plots and Guinier plots. There is a general trend for increasing molecular mass for increased generations, but there are discrepancies, such as a lower molecular mass in going from generations 1 to 2 in samples with a 50 core. Figure 8 plots the radius-of-gyration of the same samples, also showing a trend of increase with generation, but also somewhat erratic. These results, along with the lack of solubility, seem to indicate that beyond generation 1, the samples are highly nonuniform.

Figures 9 and 10 are Kratky plots of the same data in Figures 7 and 8. Kratky plots emphasize the higher q data giving information on the inner structure which is dependent on the segment density distribution. The hyperbranched and the linear samples have very similar scattering, suggesting that the hyperbranched has a relatively low degree of branching and probably a high polydispersity. The increased scattering intensity of the hyperbranched over the linear indicates that the hyperbranched has a much higher molecular mass, however. The peaks in the dendrigrafts are typical of the scattering from star-branched molecules with relatively narrow molecular mass distributions in the arms. The increase in the peak in going from G0 to G1 in both series is characteristic of an increase in the number of arms. The lowering of the peak for generations G2 and G3 is inconsistent with this increase, and is probably associated with the inconsistent results in the low angle Zimm and Guinier plots of Figures 7 and 8.

Figure 11 shows the scattering from various concentrations of PEOX(100 - 100). By 5 % a peak appears. This indicates that there is a preferred spacing of the dendrimers. This is probably due to the repulsive forces inhibiting overlap at these concentrations. The intensity and position of the peak reflect the size and regularity of the positions. Figure 12 plots the scattering from 10 % solutions of PEOX with various amounts of branching. The hyperbranched PEOX has no peak which reflects the polydispersity and low amounts of long chain branching. It is much more like the linear PEOX than the dendrigrafts. As the generation number increases, the peak becomes more intense and goes to lower angle, which is consistent with the results at low angle shown in figures 7 and 8.

PSAN was reported to be miscible with linear PEOX, so blends were made with dendrigrafts and hyperbranched of PEOX. Figure 13 shows blends with various amounts of PEOX(100 - 100). As the concentration increases, a shoulder appears in the scattering. This is probably related to the peaks that appear in the PEOX solutions, suggesting a characteristic spacing of the dendrigrafts. Figure 14 shows the scattering from 30 % blends with various types of PEOX. The hyperbranched results are characteristic of the results of linear blends, but shoulders appear in the more highly branched samples.

We should note that the lower limit of the SANS scattering data was $q = 0.007$ $Å^{-1}$ which is not small enough to give completely reliable values of the radius-of-gyration or molecular mass of large polymers, but general trends in these parameters should be valid. Since the form factors of the branched PEOX molecules are not known, extrapolation to zero angle depends on the model chosen. Two types of fits were taken on the 0.25 % solutions of PEOX in acetone-d6, Zimm plots and Guinier plots. A Zimm plot fits over a wide angular range for a gaussian structures such as a linear polymer chain, while a Guinier plot fits well for spherical structures such as dendrimers. It is likely that dendrigrafts lie between these two limits, so that the values reported here represent a possible range of values.

In conclusion, not all of the dendrigrafts could be used due to insolubility. The hyperbranched PEOX has characteristic scattering similar to linear PEOX, suggesting a low amount of long chain branching and considerable polydispersity. In going to generation 1 there is an increase in molecular mass, radius-of-gyration, amount of long chain branching, and long range order in concentrated solution. Beyond generation 1, the samples give erratic results.

Future Plans:

When replacements for the insoluble samples are obtained, the solution work will be completed, giving a complete range of dendrigrafts for structural analysis. Solutions of dendrigrafts can also be analyzed by TEM and SAXS in ways similar to the dendrimer work. The main focus of future work will be on blends of PEOX. SANS of blends with various PSAN's will map out the limits of miscibility.

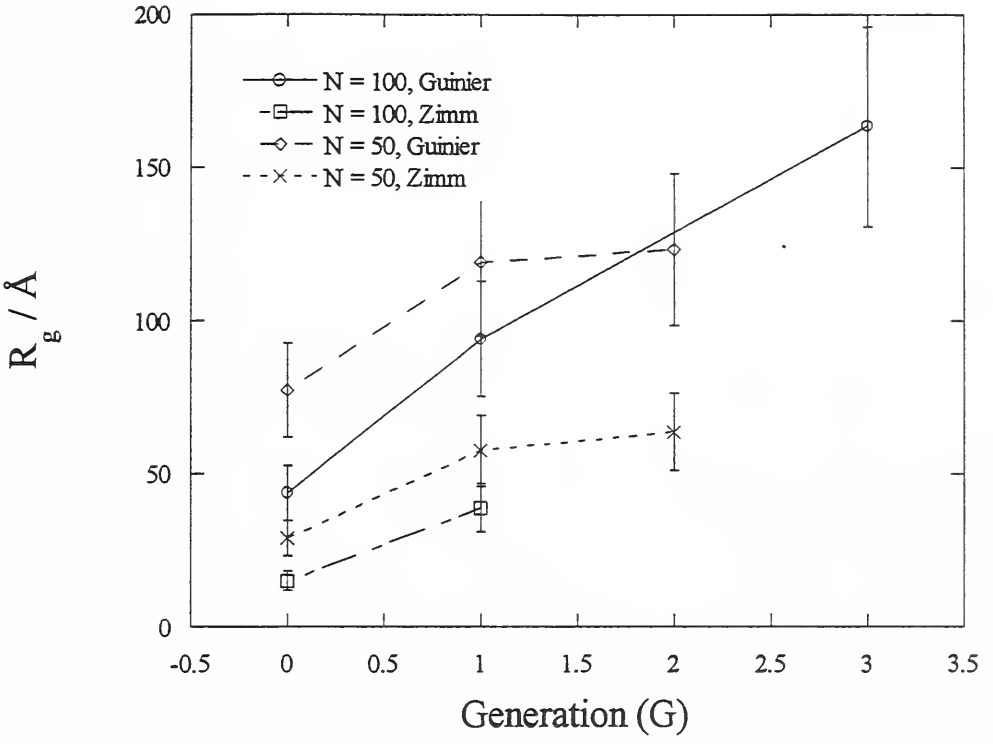

Figure 7. R_g of PEOX ($100_{(G+1)}$ – N) dendrigrafts in acetone-d6

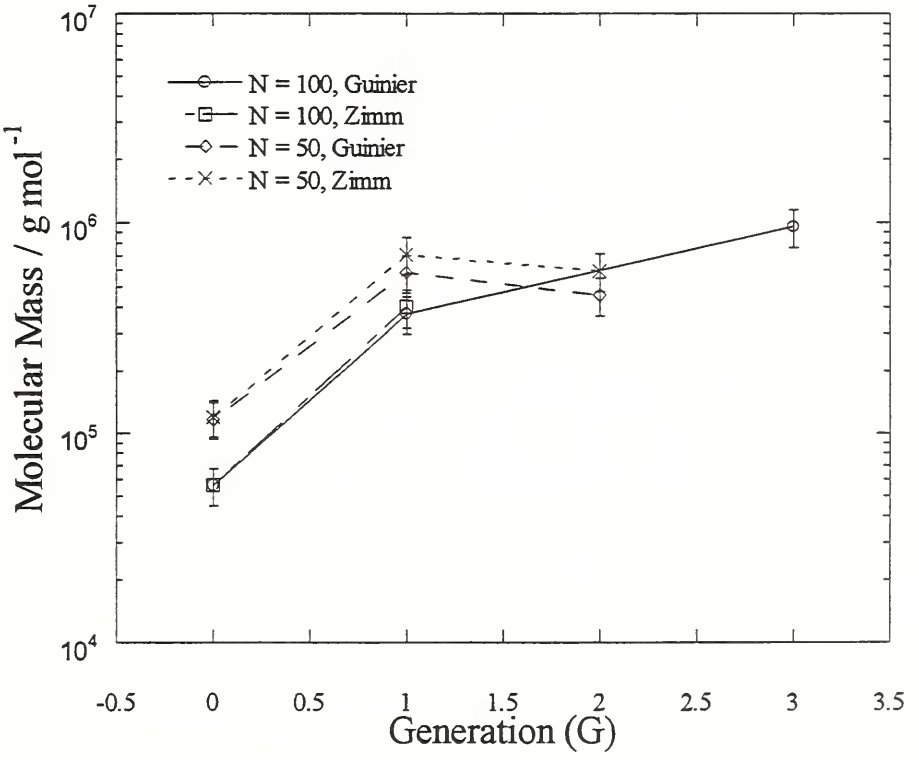

Figure 8. Molecular mass of PEOX ($100_{(G+1)}$ – N) dendrigrafts in acetone-d6.

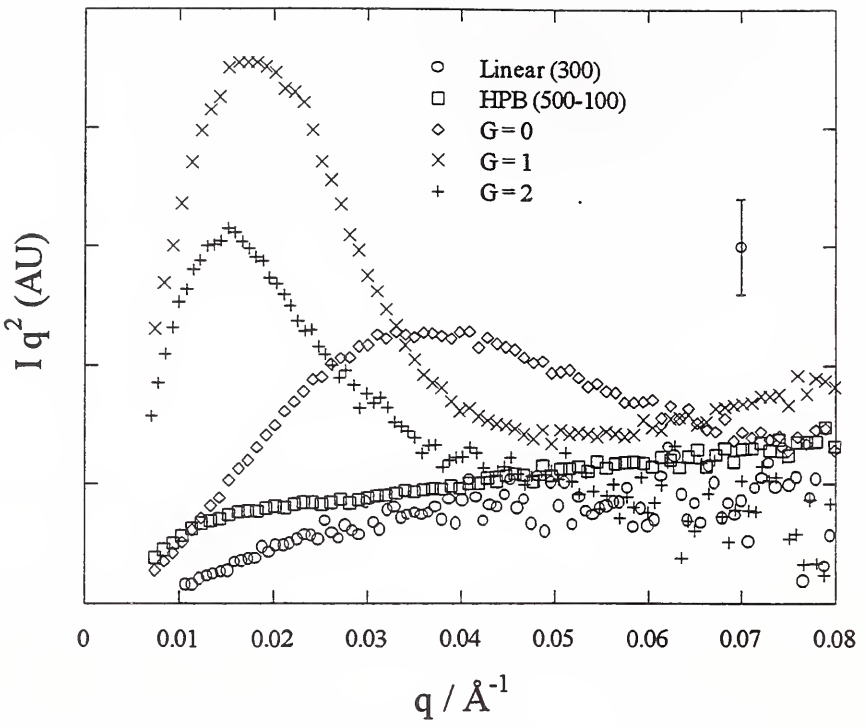

Figure 9. Kratky plots of PEOX ($100_{(G+1)}$ – 50)polymers in acetone-d6.

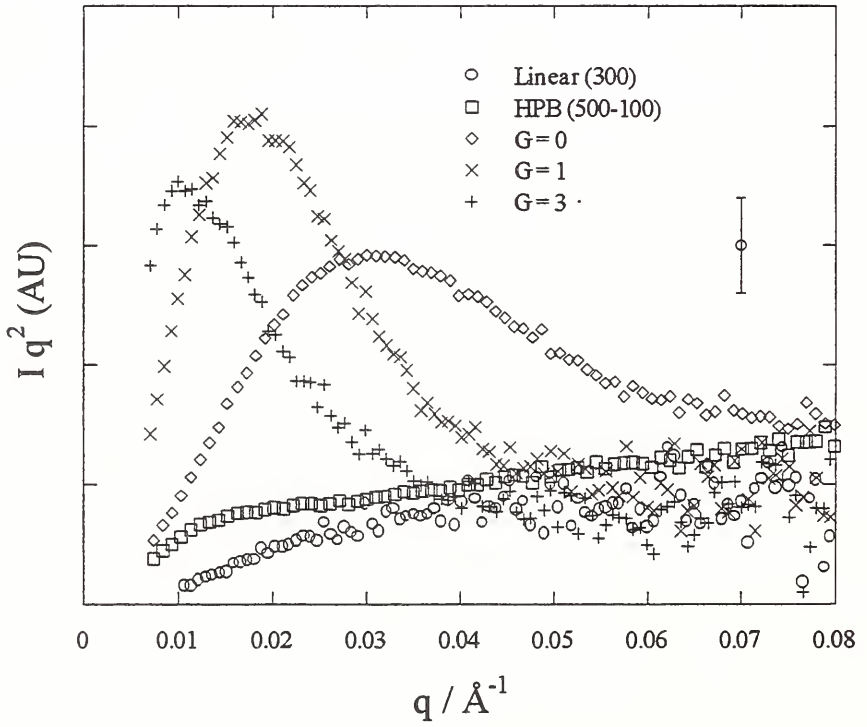

Figure 10. Kratky plot of PEOX ($100_{(G+1)}$ – 100) polymers in acetone-d6.

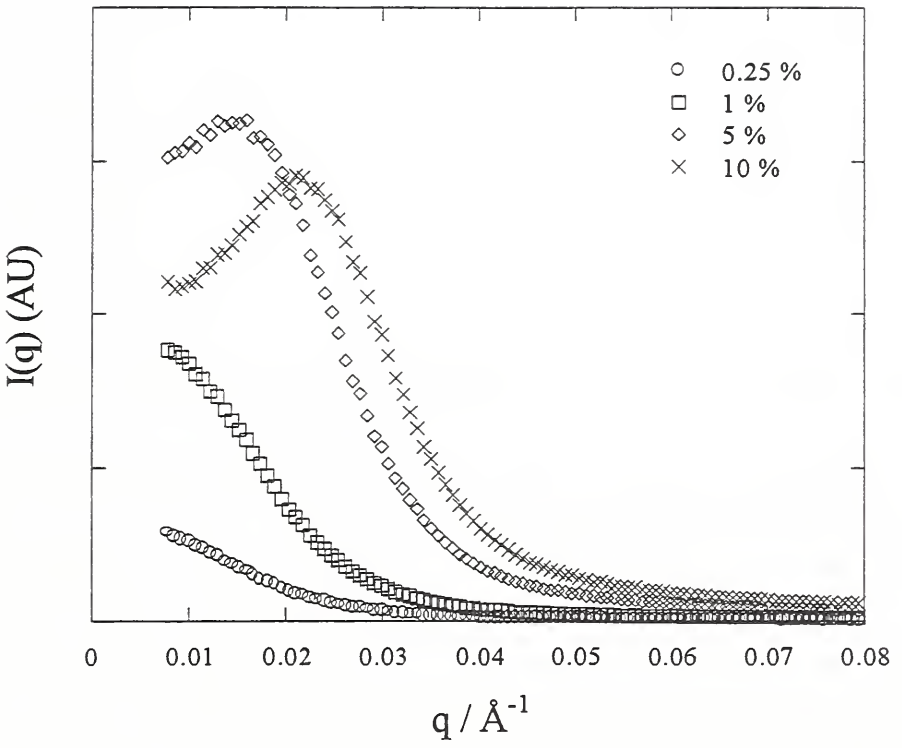

Figure 11. Concentration dependence of SANS of PEOX (100 - 100) in acetone-d6.

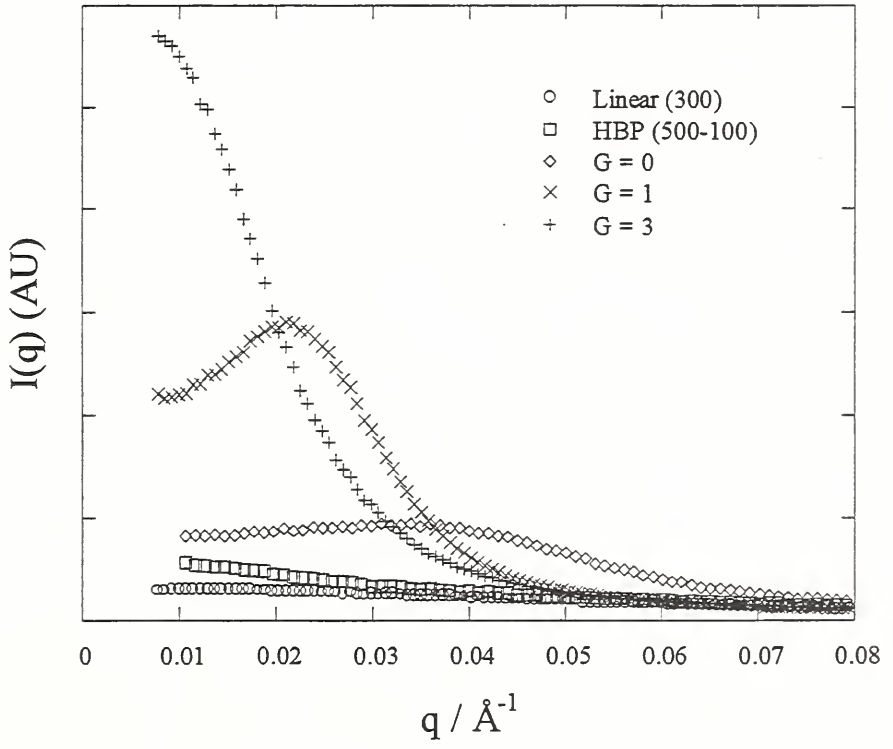

Figure 12. Generation dependence of SANS of 5 % PEOX ($100_{(G+1)}$ – 100) solutions in acetone-d6.

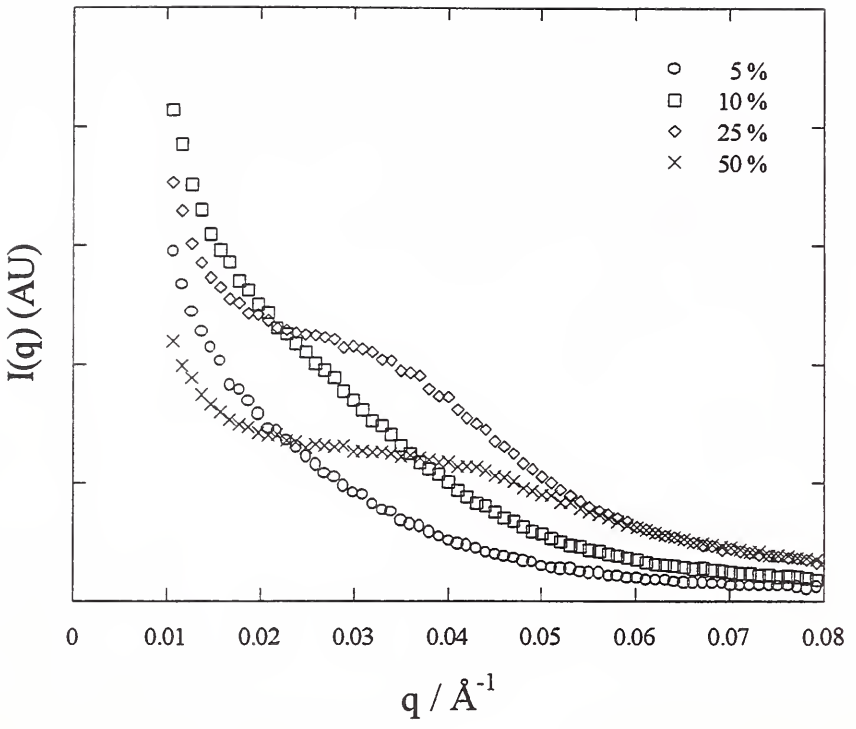

Figure 13. Concentration dependence of SANS of PEOX (100 - 100) / PSAN blends.

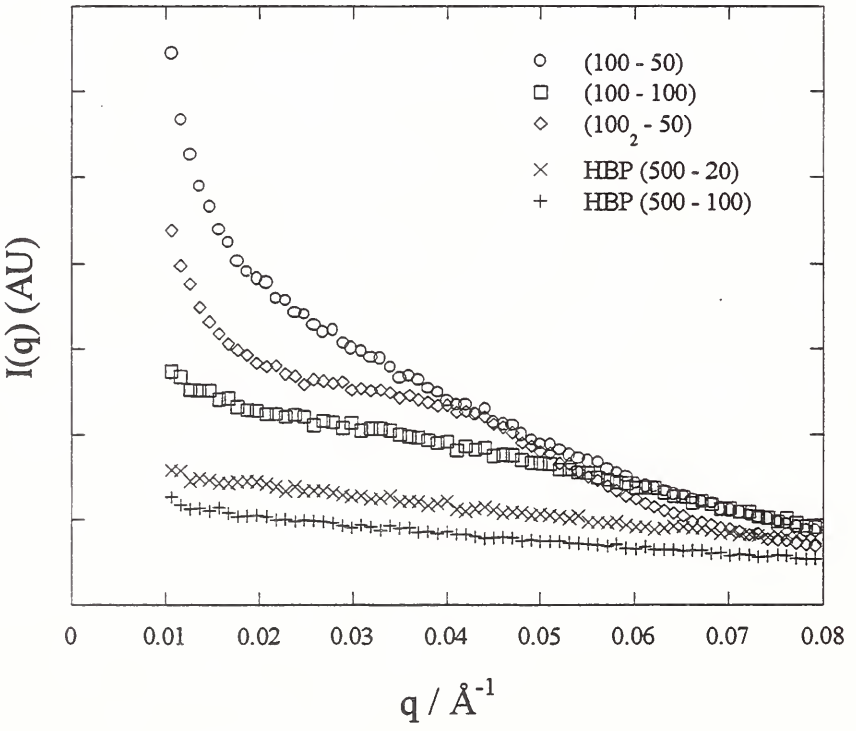

Figure 14. SANS of PEOX / PSAN blends.

SANS of PS Solutions and Blends

NIST: Andreas Topp, Barry J. Bauer, Eric J. Amis

Outside Collaborators: Mario Gauthier, U Waterloo; Sangwook Choi, U Md; Robert M. Briber, U Md.

Objectives:

To measure the size and segment density distribution of polystyrene (PS) hypergrafts in solution and in blends, and to compare them to dendrimers.

Technical Description:

SANS was used to measure the radius of gyration of PS hypergrafts generations G0 to G3 in Cyclohexane –d12, toluene-d7, and in blends with linear polystyrene-d8 (PSD).

Summary Report:

PS dendrigrafts were examined by SANS in solution and in blends with linear deuterated PS (PSD). Generations G0 through G3 were used, and all gave consistent scattering results except for generation G2. GPC was used to examine the relative molecular size to determine if the samples were consistent.

Figure 15 shows the GPC results of the four dendrigrafts along with a calibration standard. The standard has peaks for PS of Mw's 1.05×10^6, 3.3×10^5, 6.6×10^4, 9.2×10^3, and 5.8×10^2 g/mol from left to right. All samples show narrow peaks that increase in size with generation except for G2 which has a significantly smaller size. It was subsequently determined that this sample was probably not a G2 sample and has been omitted.

Figure 16 shows Guinier plots of the G3 sample in a good solvent, toluene-d8, a poor solvent, cyclohexane-d12, and a blend with PSD. The fits are all good, suggesting that the large dendrigrafts have segment distributions that are uniform and spherical. The R_g's change from the largest in the good solvent, to smaller in poor solvent, to smallest in the blend. For linear polymers, the R_g's in a Theta solvent such as cyclohexane should be the same as in the bulk. The larger R_g for the dendrigrafts in cyclohexane suggests that there has been a lowering of the Theta point, which has been previously reported. Figure 17 shows the changes in R_g with generation. The values of R_g are consistently toluene > cyclohexane > PSD.

Figure 18 shows Kratky plots of the dendrigrafts in cyclohexane at 30 °C. The higher q data probe the inner structure of the molecules. For star branched molecules, the higher the peak, and lower the drop, the more arms of the star. The peak position also shifts to

lower q with higher branching. These results are consistent with high uniformity and greatly increased branching with increasing generations.

Future Plans:

A new sample of G2 has been requested, and the SANS will be repeated to give results spanning the whole range of branching. The blend results will be fitted with the Random Phase Approximation to calculate the values of the Flory-Huggins interaction parameter as a function of branching to determine if branching enhances or inhibits miscibility.

Many blend experiments that have been done in the Blends Group with linear PS could now be continued with the PS dendrigrafts. These include:

1. Phase diagrams with PVME
2. Temperature jump experiments with PVME
3. Interfacial thickness with PMMA-d8

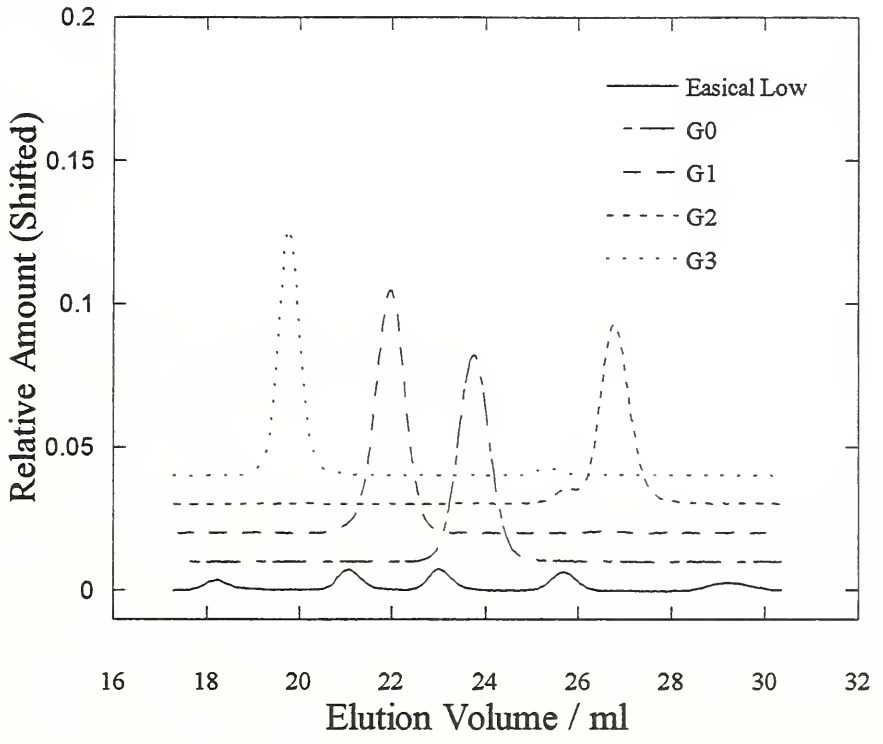

Figure 15. GPC results of PS dendrigrafts.

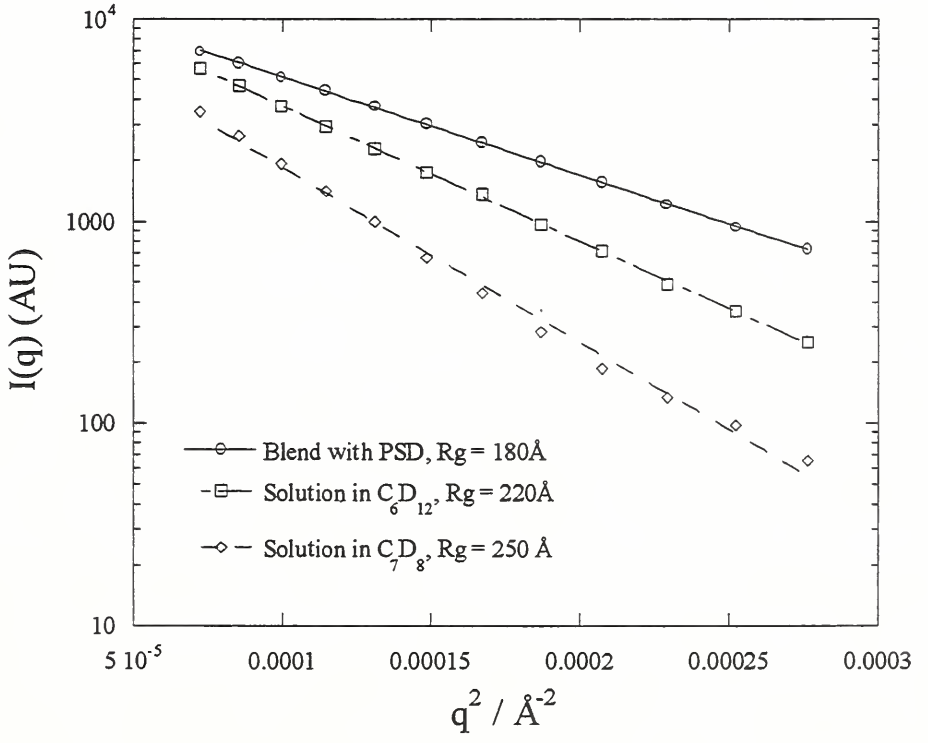

Figure 16. SANS of PS dendrigraft G3 solutions and blend.

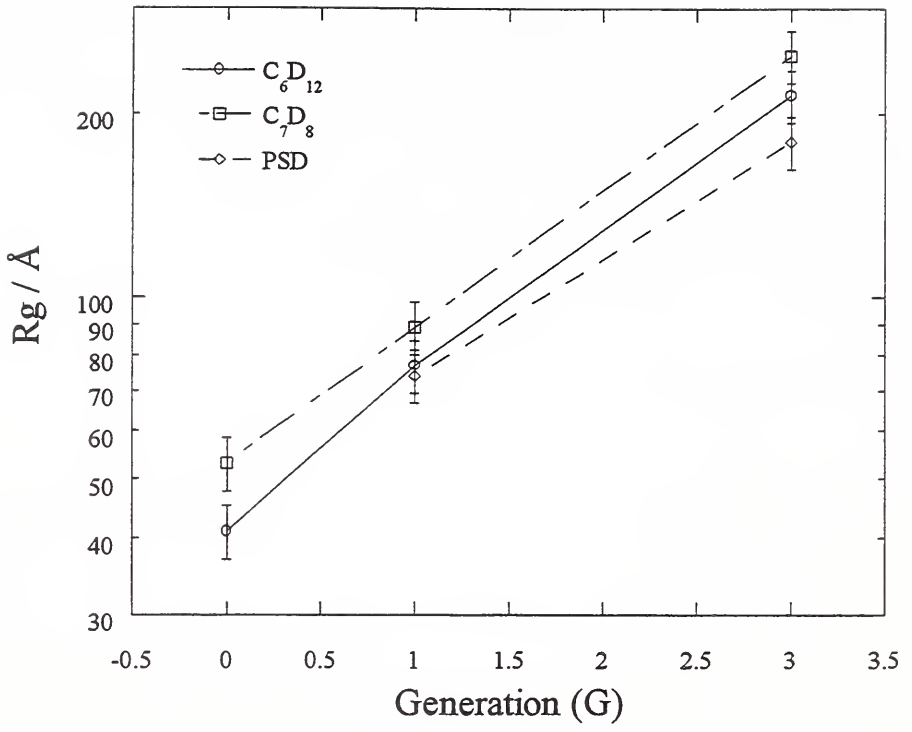

Figure 17. Radius-of-gyration of PS dendrigraft solutions and blends.

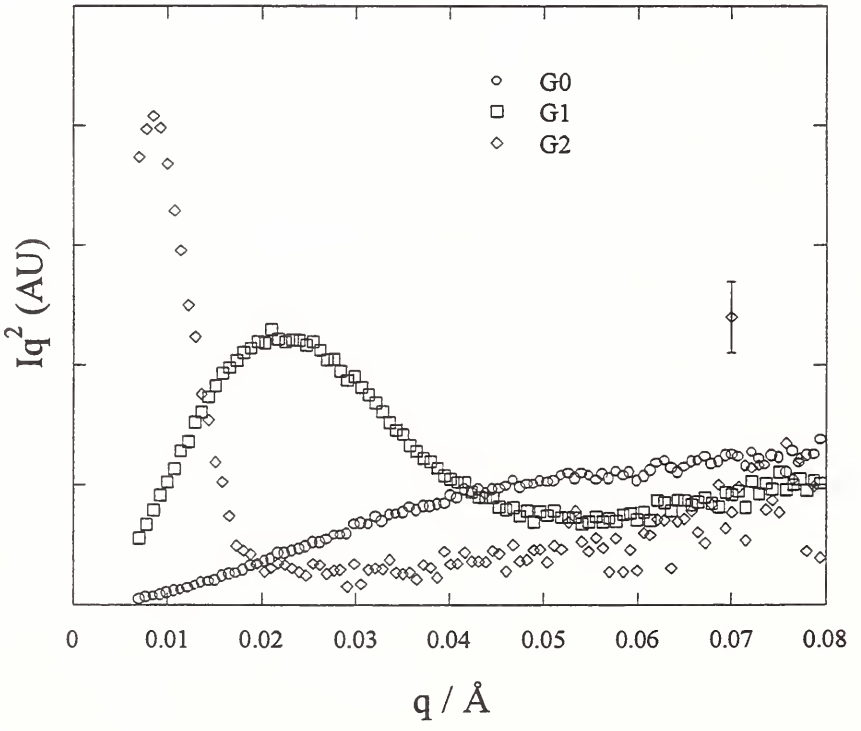

Figure 18. Kratky plots of PS dendrigrafts in cyclohexane.

Labeled PAMAM Dendrimer

NIST: Andreas Topp, Barry J. Bauer, Eric J. Amis

Outside Collaborators: Donald Tomalia, MMI; Ralph Spindler, MMI; June W. Klimash, MMI

Objectives:

To find the location of the terminal units of a dendrimer in solution and to compare their size with that of the whole dendrimer.

Technical Description:

PAMAM dendrimers were synthesized with a deuterium labeled seventh generation by use of methyl acrylate-d3. Contrast matching techniques were used to mask the earlier generations, measuring only the final generation and this was compared to unlabeled dendrimer in a high contrast solvent.

Summary Report:

The internal structure of dendrimers is of special importance for a number of different applications. In particular the potential as an agent for controlled drug delivery is based on the incorporation of a guest molecule in the interior of a dendrimer. This requires some degree of free space inside the dendrimer. A low segment density inside a dendrimer would require the segments of the last generation to be predominately located in an outer shell.

Early molecular modeling studies revealed this picture to be valid for typical PAMAM dendrimers. However, the results of kinetic growth, Monte Carlo calculations, and molecular dynamics simulation rather show a constant segment density near the core of the molecule. Also the monomers of the last generation are distributed throughout the molecule and are even found close to the core.

In this study SANS experiments are carried out with a partially deuterated PAMAM dendrimer (Generation 7) under contrast match conditions for the fully hydrogenated one. The results are compared to those from an undeuterated sample of the same generation under high contrast.

Two samples of [G7] PAMAM-Dendrimers (tetrafunctional core: EDA) are used. One is a regular dendrimer whereas the Generation 6.5 of the other is labeled with deuterium by using deuterated methyl acrylate-d_3 in the second to-last reaction step. SANS experiments with the unlabeled dendrimer were carried out under high contrast conditions in CD_3OH. The labeled dendrimer was dissolved in a CD_3OH/CH_3OH mixture that has the same average contrast as an unlabeled PAMAM dendrimer interior (60.5 % CH_3OH). In

addition, a solution of the unlabeled dendrimer in the solvent mixture is prepared to show the contrast match condition. All solutions contained a molar dendrimer concentration of approximately 1 %.

The scattering intensity for the three samples is shown in Figure 19. For the unlabeled dendrimer in the solvent mixture no curvature is present over the whole q-range, revealing contrast match conditions for the PAMAM dendrimers. The coherent scattering of the partilaay deuterated dendrimer is due only to the labeled generation (generation 6.5).

A Guinier fit is applied to calculate the radius of gyration R_g for both samples. The fits are shown in Figure 20. For the deuterated sample a larger value for R_g is obtained ($R_{g,d}$ = (41.1 ± 1.2) Å) than for the unlabeled one ($R_{g,h}$ = (34.5 ± 0.4) Å). The uncertainty in the value for the labeled dendrimer is larger due to the weak signal to noise ratio. Using the value $R_{g,h}$ to calculate the equivalent hard sphere radius of the dendrimer, a value of R_h = 44.5 Å is obtained. When the deuterated segments of the last generation are assumed to lie within a thin shell surrounding the dendrimer, the experimental radius of gyration $R_{g,d}$ = 41.1 Å is equal to the radius of the thin shell. This value corresponds well to the calculated hard sphere radius R_h = 44.5 Å for the whole dendrimer when taking into account that the deuterated segments are those of generation 6.5 rather those of generation 7. This indicates that the monomers of the last generation are preferentially located at the outside of the molecule.

For comparison the ratio between the radius of gyration for a dendrimer $R_{g'}$ and the radius of gyration for the end groups of a dendrimer $R_{e'}$ can be calculated for the model of a Gaussian dendrimer. This ratio depends on the generation of the dendrimer and can be calculated for a generation 7 PAMAM dendrimer to $R_{g'}/R_{e'}$ = 0.92. The experimental value for this ratio is $R_{g,h}/R_{g,d}$ = 0.84 ± 0.04. This again indicates that most of the end groups can be found in an outer shell, and the single dendrons have a more stretched configuration than assumed in the model of a Gaussian dendrimer.

Future Plans:

It is of interest to investigate if there are changes in the distribution of terminal units of the dendrimer going from a dilute solution to concentrated solutions and in the bulk. With the small amount of deuterated material that is currently available those experiments are limited to the bulk. We hope to be able to obtain labeled dendrimers of different size (generation) and type and continue the measurements.

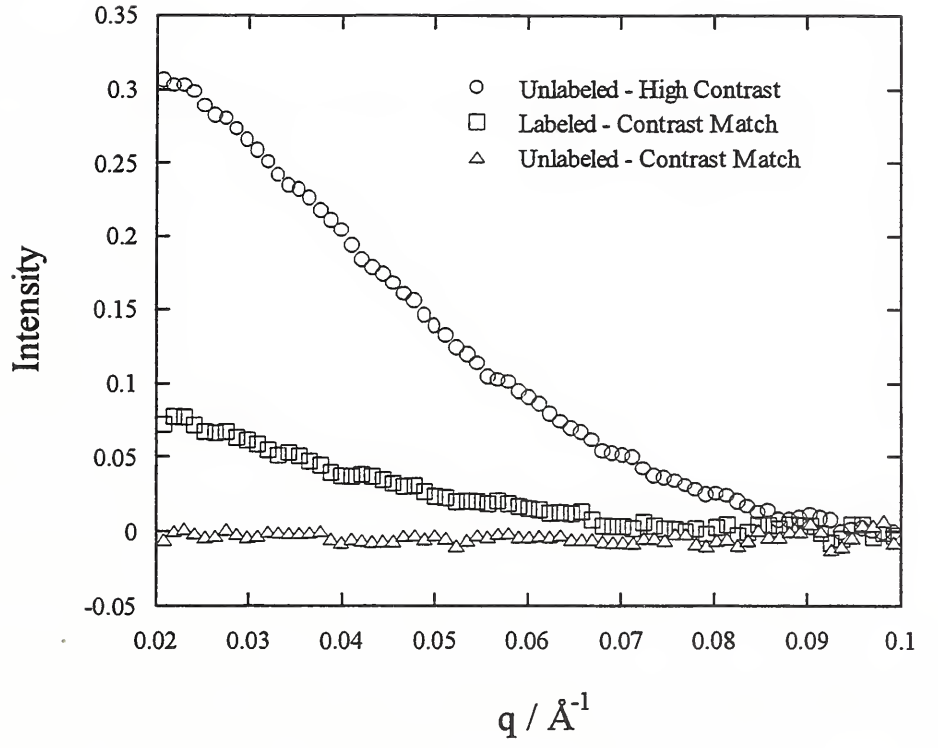

Figure 19. SANS of PAMAM G7, labeled and unlabeled.

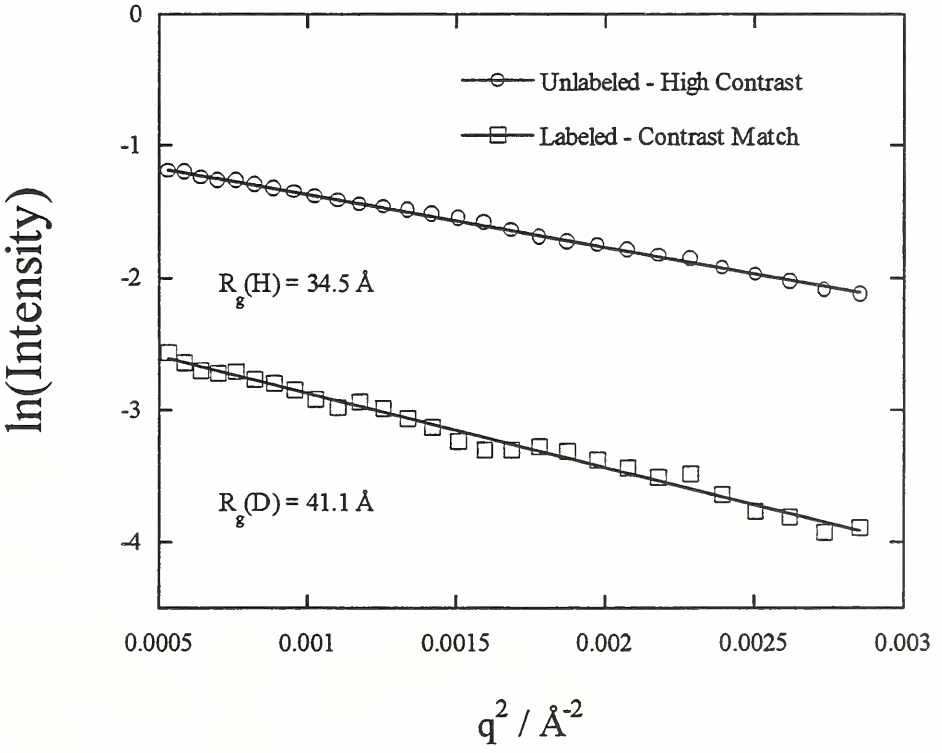

Figure 20. Guinier plots of matched and high contrast labeled PAMAM G7.

$DAB(PA)_x$ Dendrimers (DSM; x = 32 and x = 64)

NIST: Andreas Topp, Barry J. Bauer, Eric J. Amis

Outside Collaborators: Rolf Scherrenberg, DSM

Objectives:

To measure the effect of crowding on the size and amount of interpenetration of dendrimers.

Technical Description:

SANS is used to measure the amount of interpenetration of dendrimers by monitoring the size and shape of the intermolecular interference peak.

Summary Report:

The $DAB(PA)_X$ dendrimers are presently available in large quantities. Full and half generations in the range $1 \leq [G] \leq 5$ with a tetrafunctional core are produced by DSM and are now available commercially. This study deals with SANS experiments of the generations 4 and 5 that are terminated by primary amines. Compared to the classical PAMAM dendrimers that have the same terminal groups, the $DAB(PA)_X$ dendrimers have lower molecular weights and are smaller in size. Also the density in solution is higher than that of the PAMAM dendrimers.

Due to the large scale syntheses, the potential applications of these materials can be extended to those that require large quantities. This includes the use as components in dendrimer/polymer blends or in reactive dendrimer/polymer blends where the dendrimers could act as highly efficient crosslinking agent due to their high functionality. Since these dendrimers are only recently available for research, just a few studies exist that investigate the physical properties of this commercially interesting class of dendrimers. This preliminary study is concerned with the solution behavior of the generations 4 and 5 ($DAB(PA)_{32}$ and $DAB(PA)_{64}$) using CD_3OH as a solvent. The concentrations studied cover the range from dilute to high concentration solutions ($1\ \% \leq c \leq 80\ \%$).

Due to the small size of the dendrimers only the radius of gyration of the generation 5 can be determined by the SANS experiments. In Figure 21 a Guinier fit to the low-q data is shown. It results in a calculated value of $R_g = (14.8 \pm 0.3)$ Å. The weak scattering intensity for molecules of this small size and the resulting small signal to noise ratio may account for this discrepancy.

For all concentrations the scattering intensity is recorded over a wide range of the scattering vector q ($0.05\ Å \leq q \leq 0.55\ Å$). The results for the generations 4 and 5 are shown in Figures 22 and 23. The concentrations, c, are indicated as % dendrimer. With

increasing concentration a peak in the scattering intensity is observed, which has its maximum value for approximately c = 20 % concentration. For higher dendrimer content the intensity of the peak decreases and is no longer detected for at c ≥ 80 %. The peak indicates that some degree of ordering is present in the concentrated dendrimer solutions. This reveals that the dendrimers are forced to a spatial ordering by repulsive interactions, assuming that no long range interactions are present. The nature of these repulsive interactions can be explained by their tendency to avoid interpenetration of the segments from different dendrons.

A more quantitative analyses can be given assuming a cubic arrangement of the dendrimers due to the repulsive interactions. In this case the position of the peak in the scattering intensity q_{max} is connected to the mean distance Λ_{max} between the scattering centers. This distance should be in the order of 2 R_h at a concentration were the molecules approach each other closely. In Figure 24 the value Λ_{max} is shown as a function of concentration. Also shown are the values 2 R_h for the two generations studied. It can be seen that the value Λ_{max} is in the order of 2 R_h at approximately c = 20 %. For higher concentrations the value Λ_{max} is smaller than 2 R_h. This observation is consistent with the qualitative interpretation given above. The intensity of the intercorrelation peak increases for concentrations where the dendrimers do not overlap. For concentrations where the value Λ_{max} is smaller than 2 R_h the peak vanishes. It is suggested that this observation is due to the lack of repulsive forces when the segments of different dendrons interpenetrate.

For a better estimate of the value Λ_{max} ,the structure factor S(q) is calculated from the I(q) data by using the form factor P(q) of the single particle. Applying this procedure one assumes that the shape and size of the dendrimers remain constant over the whole range of concentration. Following the interpretation just given this assumption can only be valid for concentrations where the dendrimers do not overlap. The structure factors are calculated using the data from the 1 % solutions as an approximation of the form factor P(q). The resulting plots of S(q) are shown in the Figures 25 and 26. Due to the large scatter in the data for P(q) the peak positions can no longer be calculated accurately. But qualitatively it is found that the values q_{max} are shifted to lower values, resulting in smaller values for Λ. The data for S(q) of the 5 % solutions exhibit a peak that is not visible in the I(q) data.

Future Plans:

The results show that the $DAB(PA)_X$ dendrimers are, despite of their small size, suited to study the properties of dendrimers in moderately and high concentrated solutions. The results presented so far are to be considered as preliminary. The dendrimer form factor P(q) must be determined with higher accuracy in order get better results for the quantity of interest S(q). Higher q scattering in Figures 22 and 23 suggest that a higher order feature may be present. SANS or SAXS measurements may extract the size directly. Information concerning the interpenetration could also be gained from experiments with labeled dendrimers in bulk.

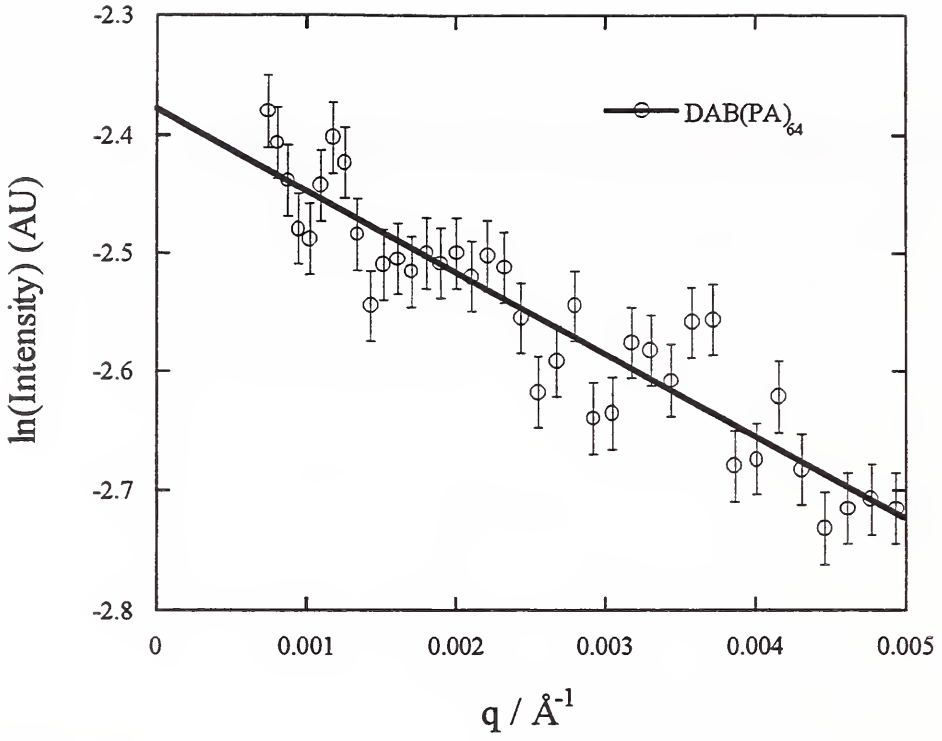

Figure 21. Guinier plot of SANS of DAB G5 dendrimer. 1 % in CH_3OH.

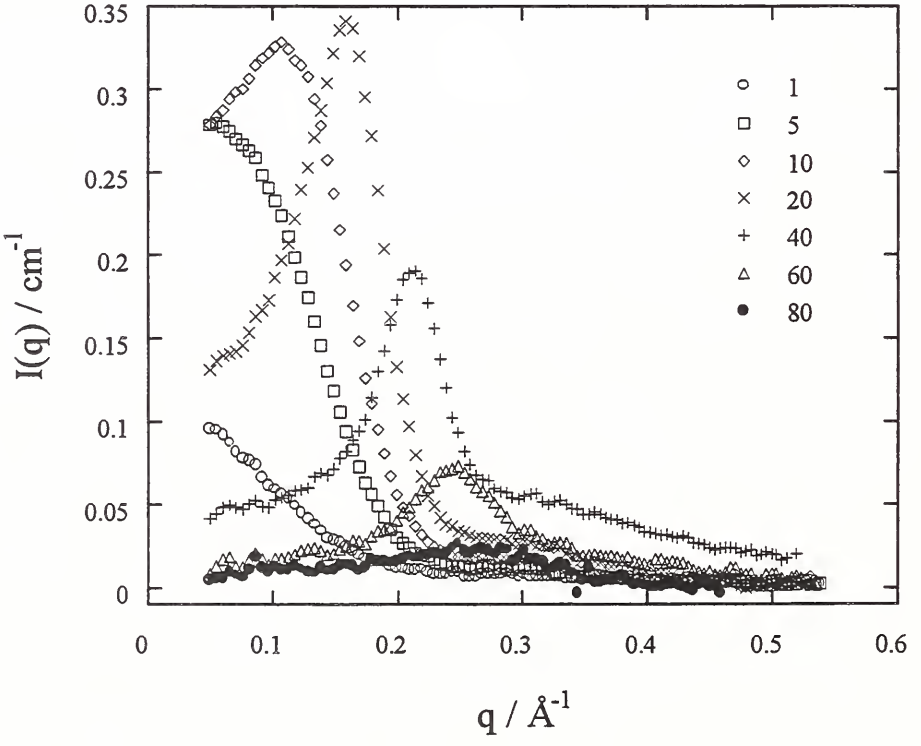

Figure 22. Concentration dependence of SANS from DAB G5.

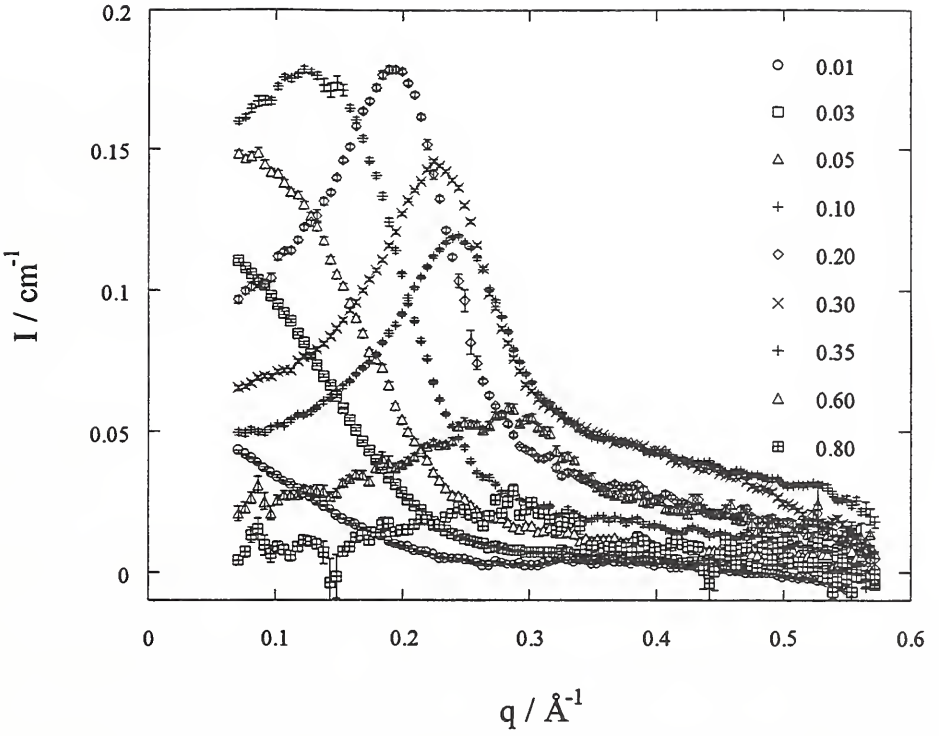

Figure 23. Concentration dependence of SANS from DAB G4.

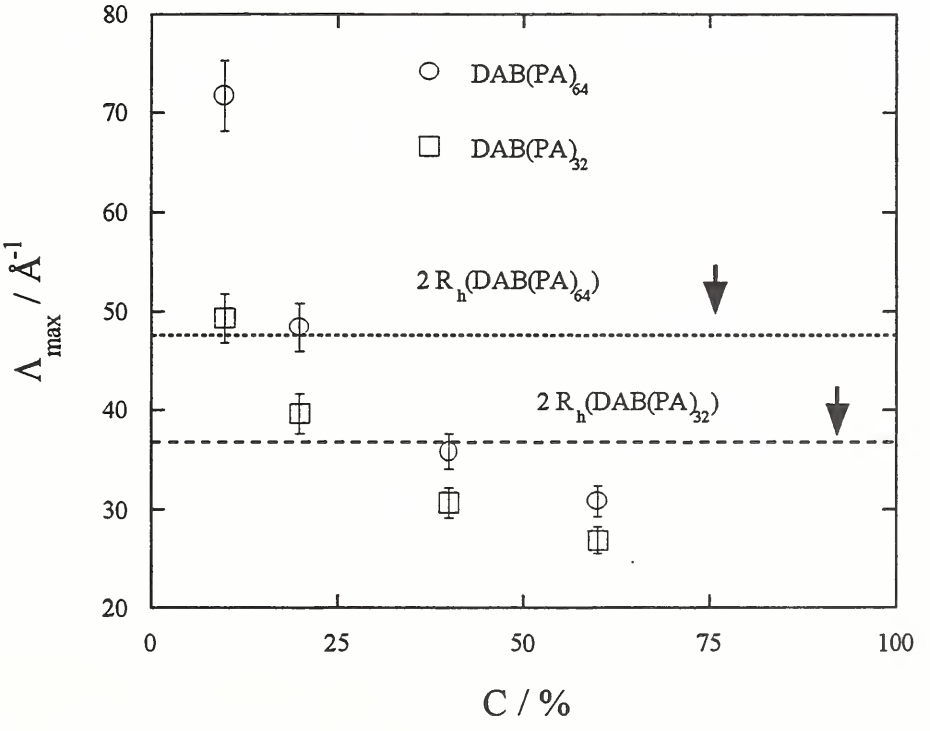

Figure 24. Concentration dependence of characteristic size from peak positions.

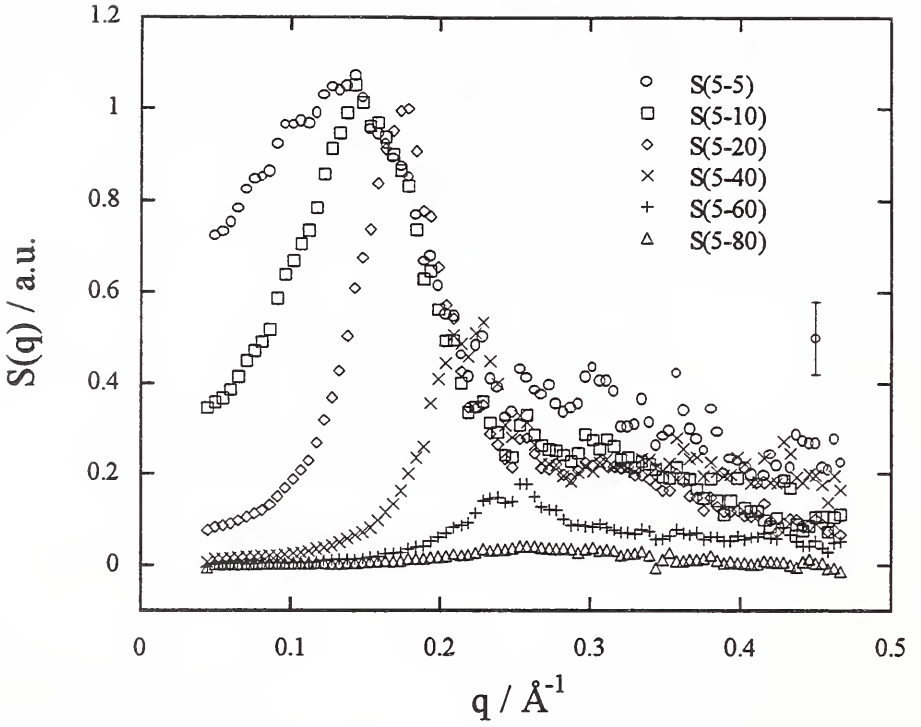

Figure 25. Concentration dependence of S(q) of DAB G5.

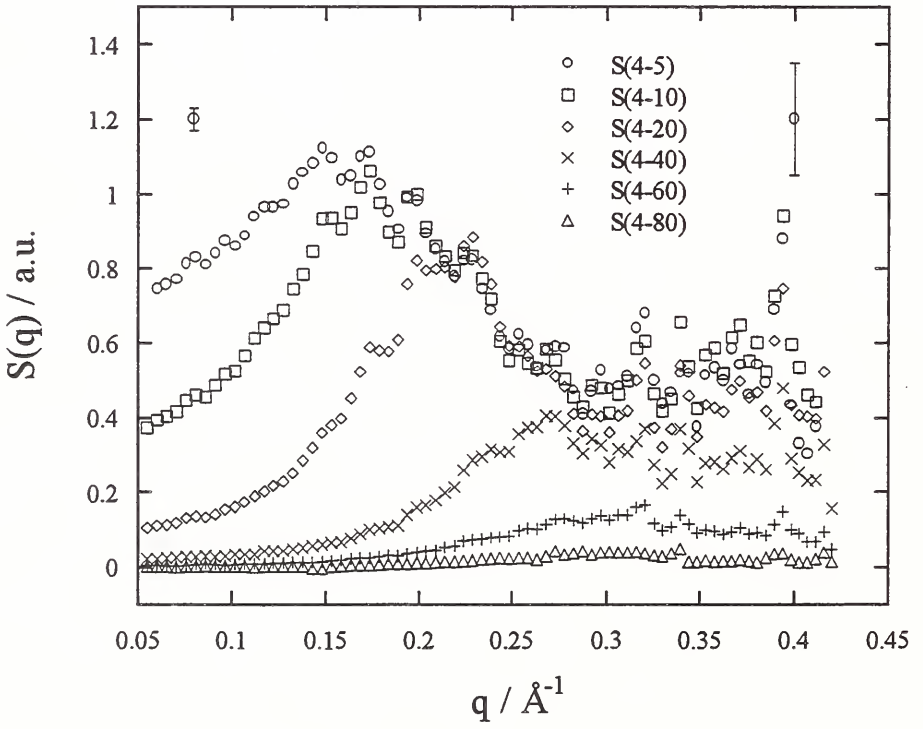

Figure 26. Concentration dependence of S(q) of DAB G4.

SANS Comparison of Hyperbranched Polymers and Dendrimers

NIST: Andreas Topp, Barry J. Bauer, Eric J. Amis

Outside Collaborators: Rolf Scherrenberg, DSM

Objectives:

To measure the relative segment density distributions of dendrimers and hyperbranched polymers of similar molecular mass.

Technical Description:

SANS of dilute solutions was used to measure single particle scattering of dendrimers and hyperbranched polyols and to compare the scattering to different models.

Summary Report:

Hyperbranched polyols and dendrimers are both highly branched structures, but the polyols are less regular molecules than the dendrimers. This polydispersity is a result of the random nature of the branching that occurs during the syntheses of hyperpranched materials. Some possible applications are the same for the two kinds of materials. Compared to the very uniform dendrimers the polydisperse materials have the advantage to be available in large quantities at low cost. Different examples of hyperbranched materials have been synthesized and various potential applications are presently being explored.

Because of the common characteristics of hyperbranched polymers and dendrimers it is of interest to study the characteristic differences between the two highly branched structures. Here, SANS experiments are carried out with solutions of two typical examples. The generation 4 and 5 of hyperbranched Perstorp Polyols are compared to a PAMAM dendrimer of approximately the same molecular mass (generation 4).

The characteristic difference in the scattering of the hyperbranched polyol (Generation 5) and dendrimer (Generation 4) are shown in Figure 27 (both are 5 % solutions in CD_3OD). The intensity is scaled in arbitrary units for a better representation. It can be seen that the scattering of the dendrimer is very close to that of a solid sphere. This behavior is seen in other SANS studies with dendrimer solutions and is also observed with SAXS experiments. The scattering from the polyols is different from that of a solid sphere. It is close to the typical scattering observed with polydisperse polymers.

The difference, as found in the scattering behavior, is consistent with the molecular characteristics of the different species. Dendrimers, at least the smaller generations, have an extremely narrow molecular mass distribution. The perfect architecture of the different dendrons then leads to a very uniform shape. The hyperbranched systems have not only a high degree of polydispersity in terms of molecular mass, but also a polydispersity in

terms of the shape of the molecule. This difference is seen in the SANS results and is an important consideration for the calculation of molecular dimensions from scattering experiments.

Figure 28 is a Guinier plot for solutions of the polyol (Generation 5) and the PAMAM dendrimer (Generation 4). It is obvious that there is a strong curvature to the data of the polyol whereas the linear region for the dendrimer is extended to very high q values. This is consistent with the spherical shape of the dendrimer, for which the Guinier approach should give accurate numbers. For the polydisperse and nonuniform polyol, deviations from a straight line in a Guinier representation are expected and obviously present. This data should be represented as a Zimm plot, which is the other commonly applied procedure to determine molecular parameters. As can be seen from Figure 29, a straight line is obtained in the 1/I versus q plot for the polyol, whereas the data for the dendrimer are not linear, even at very low q. This again confirms the difference between the two highly branched materials and is due to the difference in shape and polydispersity.

Calculation of numbers for the radius of gyration for the two species is done by applying a Guinier and Zimm type of fit. It is consistently found that the Guinier fit results in lower values of R_g than the Zimm plot. It has to be kept in mind that the Guinier fit does not give stable values for the hyperbranched polyols because of the curvature over the q range used for the fit ($0.02\ Å \leq q \leq 0.055\ Å$). The opposite is true for the values extracted from a Zimm plot. The numbers determined in this study are given in Table 2.

Future Plans:

The internal structure will continue to be explored for all new types of branched polymers obtained. Both SANS and SAXS will be used where appropriate. The scattering will be compared to the calculations from model distributions.

	GUINIER R_g / Å	ZIMM R_g / Å
G4 Polyol	21 ± 2	31 ± 3
G5 Polyol	25 ± 2	34 ± 3
G4 PAMAM Dendrimer	13 ± 2	13 ± 2

Table 2. Values for the radius of gyration R_g determined from SANS by different fits.

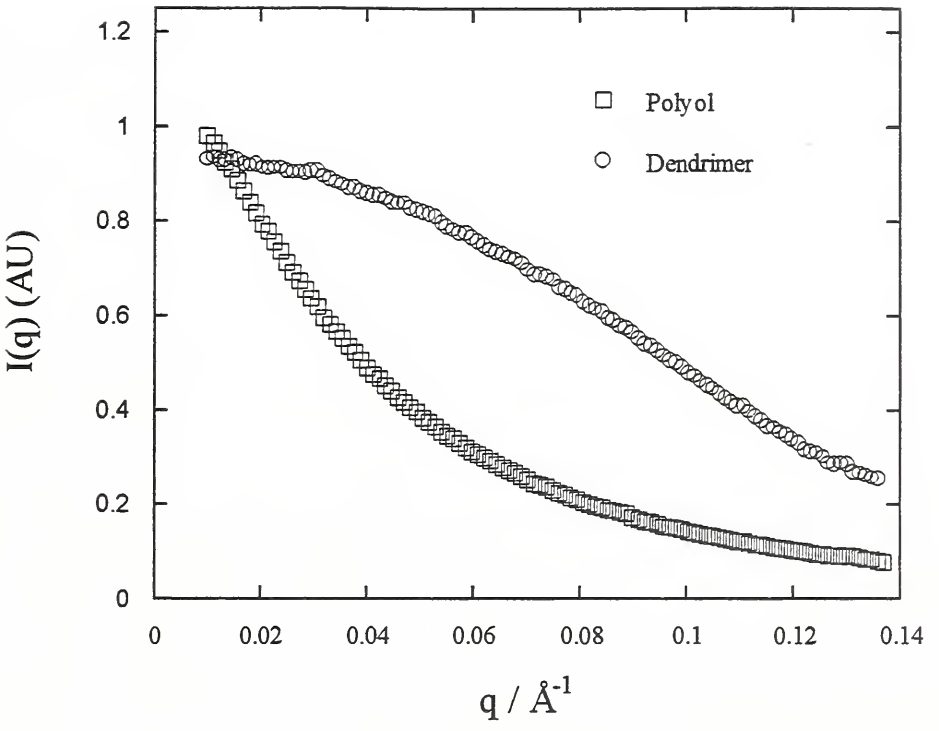

Figure 27. SANS of PAMAM G4 and polyol hyperbranched G5.

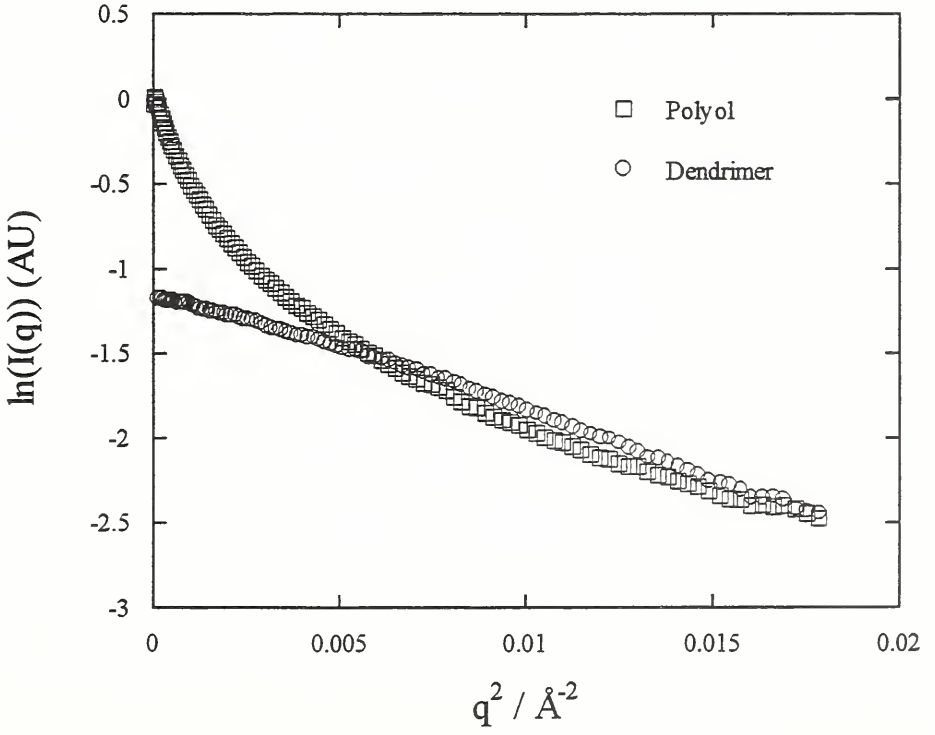

Figure 28. Guinier plot of SANS of PAMAM G4 and polyol hyperbranched G5.

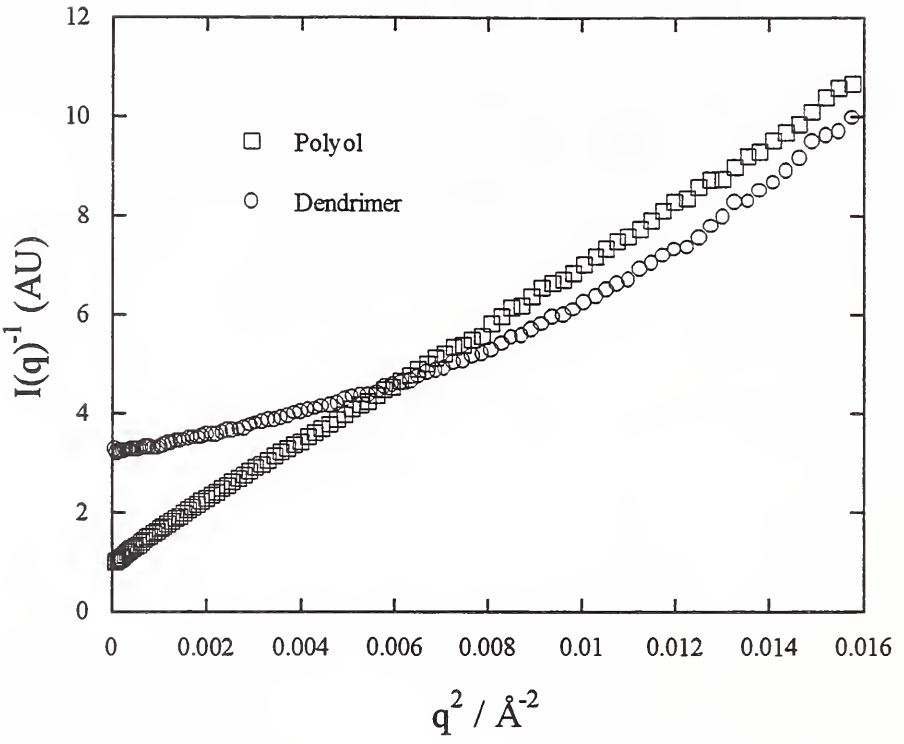

Figure 29. Zimm plot of SANS of PAMAM G4 and polyol hyperbranched G5.

Hybrid Linear-Dendritic Block Copolymers

NIST: Andreas Topp, Barry J. Bauer, Eric J. Amis

Outside Collaborators: Ivan Gitsov, Cornell U; Jean M. J. Fréchet, Cornell U

Objectives:

To measure the change in size and associations of hydrophylic-hydrpophobic dendrimer-linear polymer triblocks in selective solvents.

Technical Description:

SANS was used to characterize PEO capped with poly benzyl ether dendrons of various molecular weights in tetrahydrofuran-d8 (THF) and D_2O/methanol-d4 at various concentrations to measure the change in size and association.

Summary Report:

Associative polymers have hydrophylic and hydrophobic blocks that form hydrophobic complexes in water based solvent mixtures. The rheological properties are strongly affected by the types of associations which can be probed by small angle scattering.

The hybrid linear-dendritic ABA copolymers consist of stiff dendritic aromatic polyethers as block A that are connected via a flexible linear block B of polyethylene oxide (PEO). Six samples were studied that were built by a combination of dendrons ([G2] or [G3]) and linear PEO, M_w, (11, 15 , and 23) kg/mol. Two different solvents were used, one of which (THF-d8) is a good solvent for the dendrons and a bad solvent for the PEO chain. The other solvent used is an equal volume mixture of CD_3OD/D_2O. This mixture is known to be a good solvent for PEO, but is a nonsolvent for the dendrons.

The SANS experiments reveal that the ABA copolymers dissolved in THF-d_4 form a solution of single particles (see Figure 30). This suggests the formation of intramolecular micelles formed by the dendrons (blocks A) that are surrounded by the freely soluble PEO chain (block B).

In contrast to the THF-d8 solutions, the copolymers form gels in the mixture CD_3OD/D_2O for concentrations $c \geq 3$ %. For concentrations of $c = 15$ % the gels are macroscopically stable and do not flow over a time period of days. In the SANS results the gelation is reflected by the appearance of a maximum in the angular dependence of the scattering intensity I(q). This maximum is first observed for a concentration of $c = 3\%$ as can be seen in Figure 31.

For the macroscopically gelled samples a higher order feature shows up in the Kratky plot. This is shown in Figure 32 for the samples composed of two [G3] dendrons and different molecular masses of the PEO chain. The peak reflects a regular ordering of

micelles formed by the dendrons. The formation of micelles is due to their hydrophobic interactions in the solvent mixture. The strongly uniform spacing between the micelles, as indicated by the narrowness of the observed peak, and the presence of a higher order shoulder, can be explained by an idealistic model consisting of dendrons of one ABA copolymer that are located in different micelles that are bridged by the PEO chain. However, because of entropy it is more likely for real gels that bridged micelles coexist with those that are not bridged.

Future Plans:

Associations of the blocks in solvents selective for the PEO or the dendrons will be studied by SANS to measure the micellar sizes.

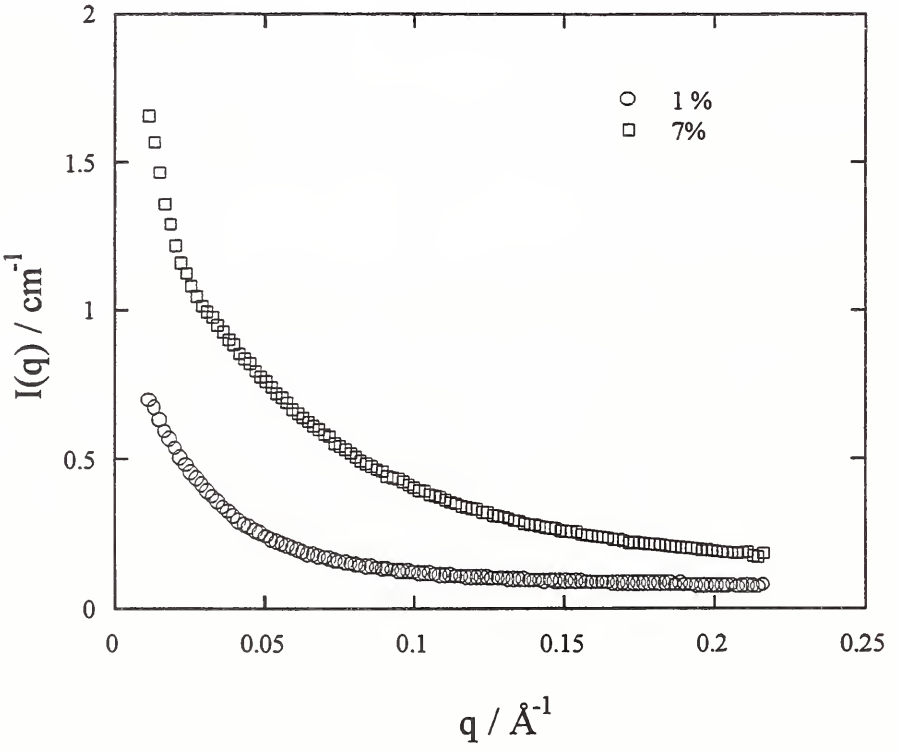

Figure 30. SANS of concentration dependence of ABA Dendritic copolymer in THF-d8.

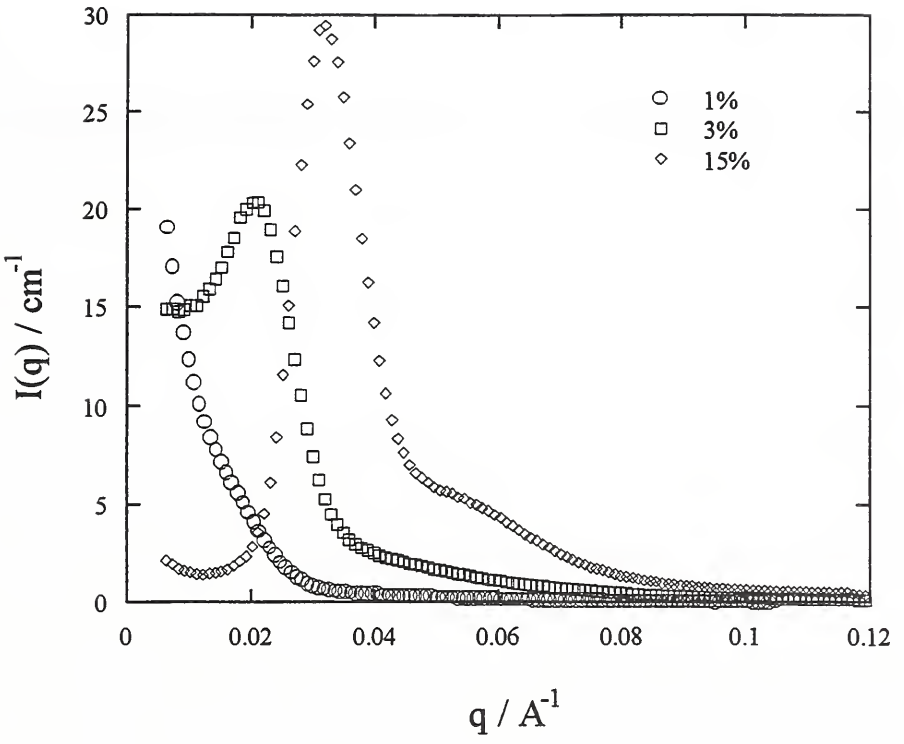

Figure 31. SANS of concentration dependence of ABA Dendritic copolymer in D_2O/CD_3OD.

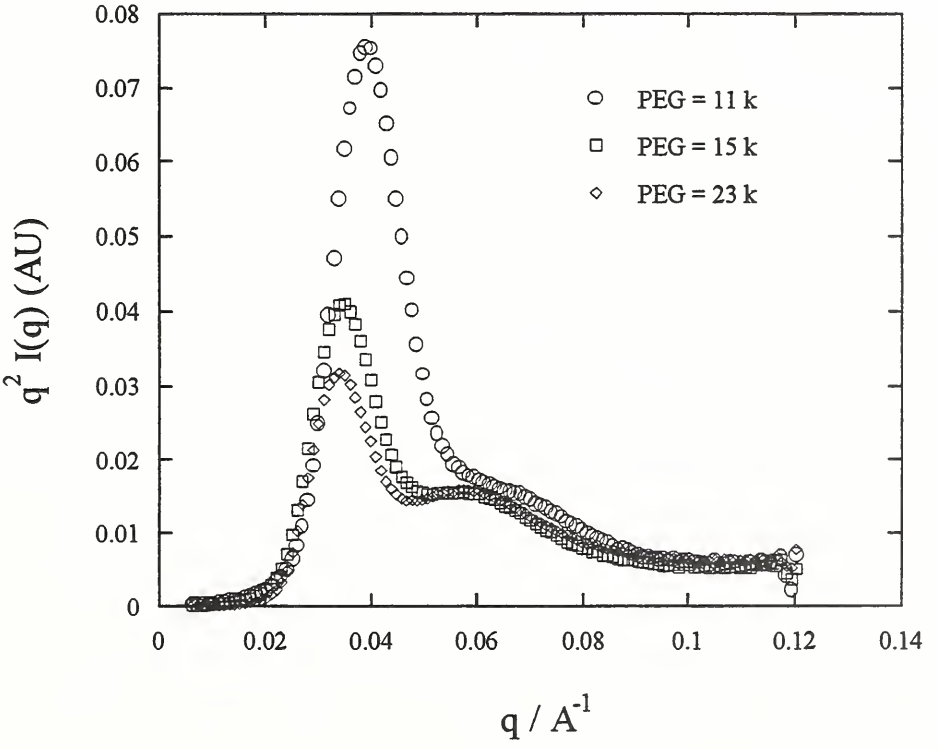

Figure 32. SANS of B block Mw of ABA Dendritic copolymers in D_2O/CD_3OD

SAXS Measurements of Various Dendrimeric Materials

NIST: Ty J. Prosa, Barry J. Bauer, Eric J. Amis

Outside Collaborators: Donald Tomalia, MMI; Rolf Scherrenberg, DSM; Jean-Pierre Majoral, CNRS

Objectives:

To develop a routine characterization technique for the size and segment density distribution of dendritically branched materials. To compare the sizes of dendrimers and hyperbranched molecules of various types and generations.

Technical Description:

SAXS has been used to characterize dendritically branched materials by using naturally occurring contrast in standard solvents and various scattering models have been applied to model the SAXS curves.

Summary Report:

A number of SAXS measurements were performed on various dendrimeric systems including PAMAM, DSM, and phosphorus dendrimers, Polyol hyperbranched, and PEOX dendrigrafts. All measurements reported below were done at the NIST SAXS facility operating primarily in the 5 meter configuration.

The main limitation in determining R_g (radius of gyration) for the various materials is the determination of appropriate SAS backgrounds due to the main beam, kapton solution cell windows, and scattering by the solvent. Evaporation of solvent as well as swelling of the kapton cell windows during data acquisition made the determination of all background subtractions via transmission coefficients non- trivial. This problem had its strongest influence on intensity at low values of q, and strongly influenced observed limiting power law behavior.

R_g 's were determined from Guinier plots of corrected SAS curves at q values ≥ 0.015 $Å^{-1}$. For the largest PAMAM dendrimers, the strength of dendrimer scattering at low q resulted in curves that were insensitive to background subtraction thus providing a relatively reliable Guinier region for R_g determination. The additional presence of high order scattering structure allowed simple comparisons with spherical particle scattering factors. General agreement between the two values of R_g was extremely good. For smaller PAMAM dendrimers, and all the other dendrimers reported here, the subtraction of scattering background limited the reliability of intensities at low values of q. For these systems, the limiting slope of the lowest reliable values was used to determine R_g via a Guinier plot. R_g values are included in Table 3 and Figures 33 and 34. Plotted error bars were based on a combination of known limitations in R_g values determined via Guinier

plots and the general quality of data in the Guinier region. Data with significant backgrounds have been given larger error bars when appropriate.

Single particle scattering factors for PAMAM dendrimers from G3-G10 were determined from 1% PAMAM/MeOH solutions by weight. These scattering factors are consistent with scattering from monodisperse, sphere-like objects that have radii which grow "linearly" with generation. The higher generation dendrimers (G7-G10) exhibit higher order features indicative of large spheres with monodisperse particle size and shape distributions (note that the radius of a sphere of constant electron density is related to R_g by $R_g = 0.6^{1/2} R_{sphere}$). The smaller generation dendrimers have scattering curves that have qualitatively the same shape as the larger dendrimers, except that there are no clear higher order features observed in their measured scattering profiles. The presence of distinct, higher order features is strong evidence for mondispersity of molecular size and shape. For intermediate and small sized dendrimers, it is unclear whether these features truly are not present, or if the statistics are too poor to resolve them. For the smallest generations, limitations in the range of q also effects the ability to measure the presence/absence of higher order features. Future experiments are indicated to resolve these questions.

Figure 35 is a master curve of the individual dendrimer scattering curves in arbitrary units, and scaled by R_g. This highlights the qualitative agreement between scattering factor shapes for dendrimers G3-G10, thus implying a progression of similar particle shapes with growing radii as a function of dendrimer generation.

Single particle scattering factors of PAB dendrimers from G3-G5 were determined from 1% PAB/MeOH solutions by mass (G2 was too small to measure adequate signal for reliable R_g determination). Because of the small size of these lower molecular mass dendrimers, the overall SAXS signal is relatively weak. Resulting scattering curves are consistent with sphere-like particle scattering observed in the above PAMAM dendrimers. The resulting R_g 's are comparable to measured R_g's for PAMAM dendrimers with similar molecular mass (see Tables 3 and 4 and Figures 33 and 34). However, these R_g values are consistently smaller than the values determined by SANS, which in turn are smaller than DSM's reported values. Because of the extremely weak scattering from these small sized molecules, the absolute magnitude of these reported R_g's come into question. Small variations in solvent and window subtraction greatly effect the slope of resulting Guinier plots. The general trends for the three PAB R_g's reported here can generally be considered more reliable because of the consistent treatment of all three generations. For these reasons, the error bars for these R_g values in Figures 33 and 34 are larger than the other reported R_g values.

Two phosphorus containing dendrimers were recently received from Dr. Jean-Pierre Majoral and were dissolved to make 1 % solutions in acetone by mass. The two slightly different G4 materials had R_g's that correspond favorably in size to G5 PAMAM which has a similar molecular mass (see Table 4 and Figure 34).

Single particle scattering factors of Polyol hyperbranched from G2-G5 were determined from solutions of 1% Polyol/MeOH. The molecular mass of these materials are comparable to PAMAM Dendrimers of 1 lower generation. Figure 36 contains plots of both 1% and 5% G4 PAMAM/MeOH dendrimer solutions and both 1% and 5% G5/MeOH hyperbranched solutions all of comparable molecular mass. The solvent removed scattering of the hyperbranched material is qualitatively different from that of the dendrimer scattering. The PAMAM dendrimers have scattering that is more Gaussian in shape verses the exponentially decaying shape of the hyperbranched material's scattering. The likely presence of polydispersity in the hyperbranched contrasted with the mondisperse nature of the dendrimer is likely to strongly influence these different scattering shapes.

Figure 37 shows the scattering from dilute and more highly concentrated solutions of PAMAM G10 in methanol. Higher order features in the scattering can be clearly seen in both, and the positions are unchanged. This suggests that the size of the individual dendrimers is unchanged up to 26 %. Therefore SAXS of dendrimers at even higher concentrations may be able to resolve the question of whether dendrimers overlap or shrink when they are forced together.

Future Plans:

The AP-PRT beamline at Brookhaven will allow for more types of experiments due to the significantly higher beam intensity. Several projects can be extended or initiated such as:

1. Better statistics can be obtained at higher q to investigate the internal structure of dendrimers in more detail and fitted to various models.
2. The size of dendrimers at high concentration can be measured from the location of higher order features.
3. Dendrimers with bonded or chelated metals can be examined to determine the extent and location of the attachment.
4. The weak contrast of materials such as IPNs may be enough for study at Brookhaven.

Generation	PAMAM.	PAB.	MCP.	Polyol.
G2				13.4
G3	13.8	6.2		20.5
G4	17.1	8.9	23.3,20.3	27.4
G5	23.8	10.6		31.5
G6	28.0			
G7	33.7			
G8	42.4			
G9	49.1			
G10	56.6			

Table 3. Radius-of-gyration in Å of dendrimers and hyperbranched molecules of various types as a function of generation. Standard deviations of the fits are typically ± 5 % of the given value.

Generation	PAMAM	PAB	MCP	Polyol
G2				1.73
G3	6.9	1.69		3.57
G4	14.2	3.51	26.7,29.7	7.25
G5	28.8	7.12		14.6
G6	58.0			
G7	116			
G8	233			
G9	467			
G10	934			

Table 4. Molecular mass in kg/mol of dendrimers and hyperbranched molecules of various types as a function of generation as reported by the manufacturer.

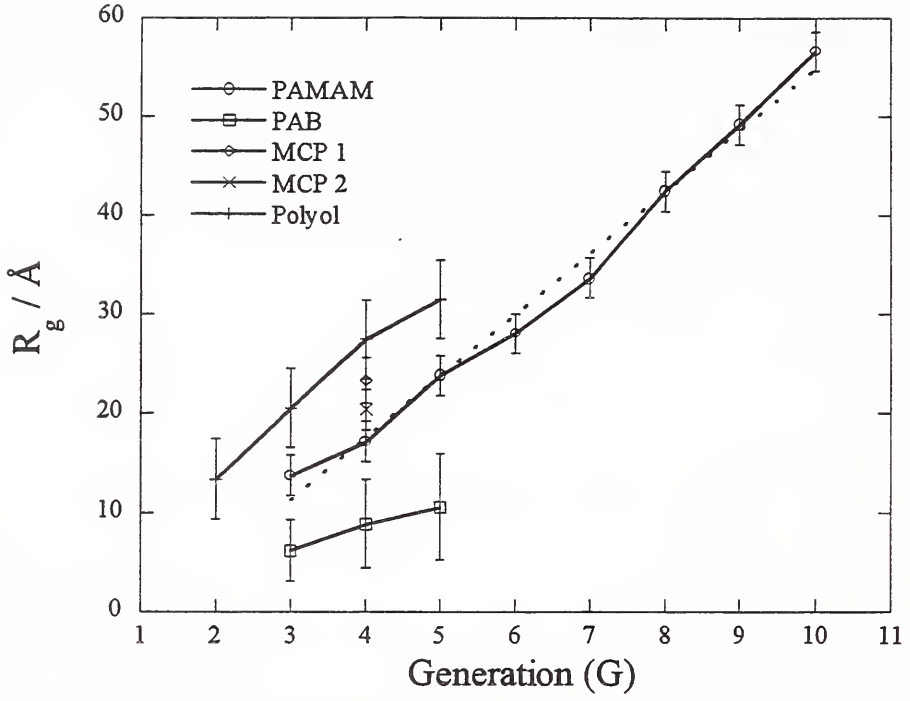

Figure 33. Generation dependence of R_g of various dendritic molecules.

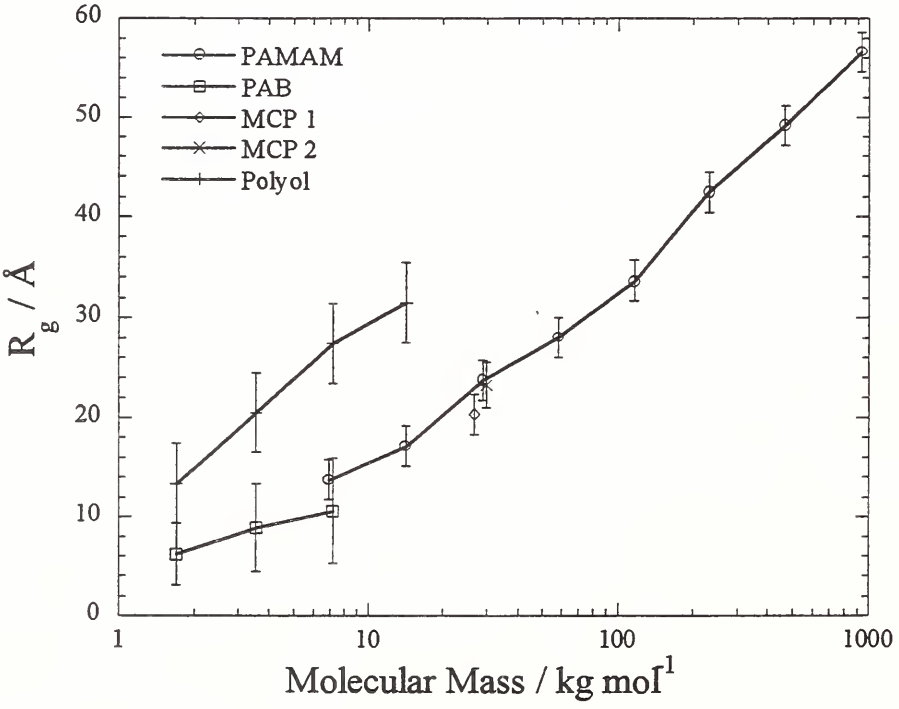

Figure 34. Molecular mass dependence of R_g of various dendritic molecules.

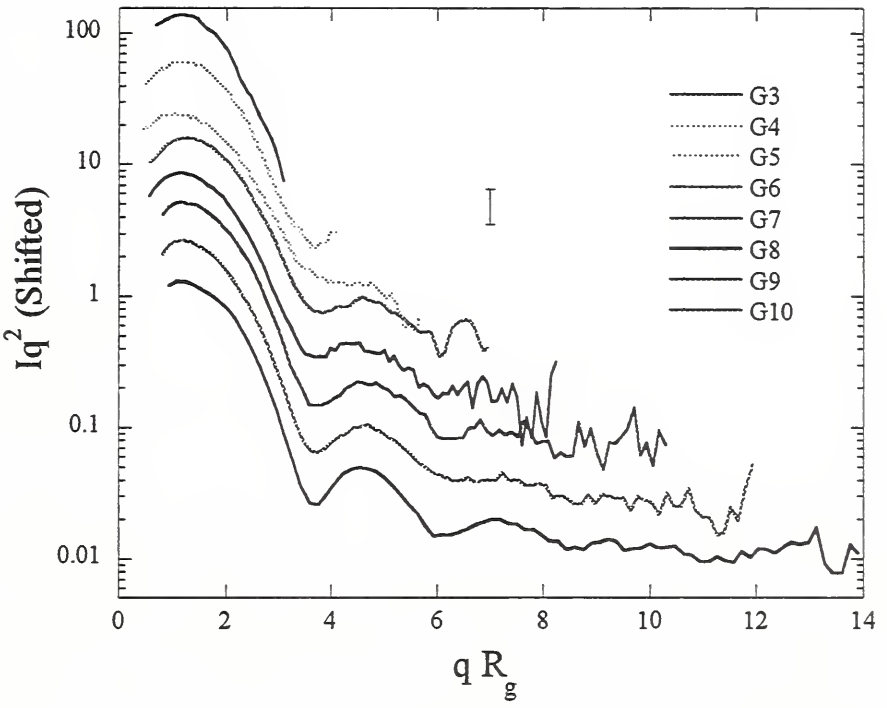

igure 35. Kratky plots of SAXS of PAMAM dendrimers.

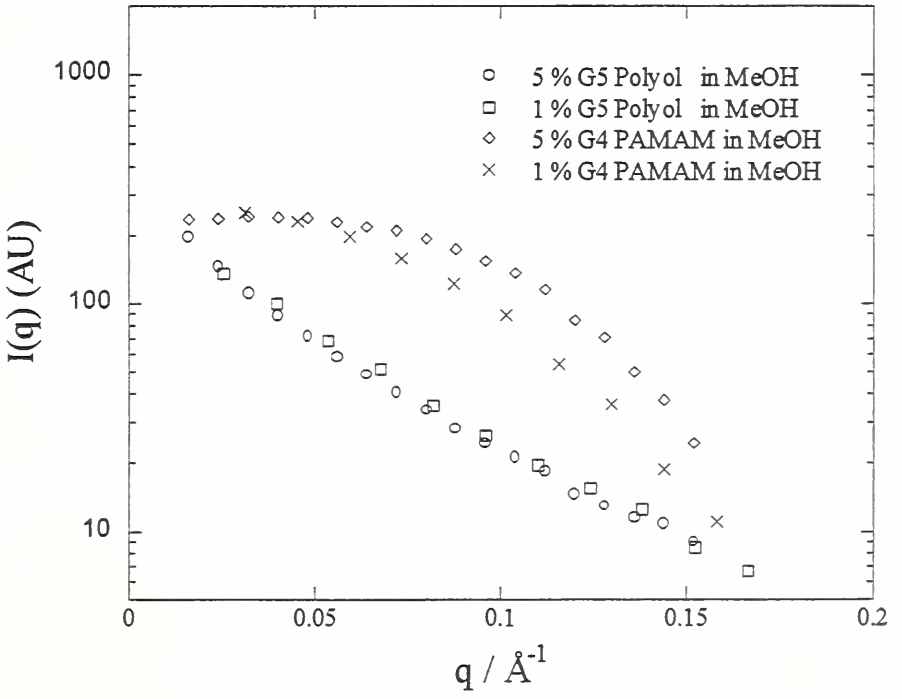

Figure 36. SAXS from PAMAM G4 and hyperbranched polyol G5.

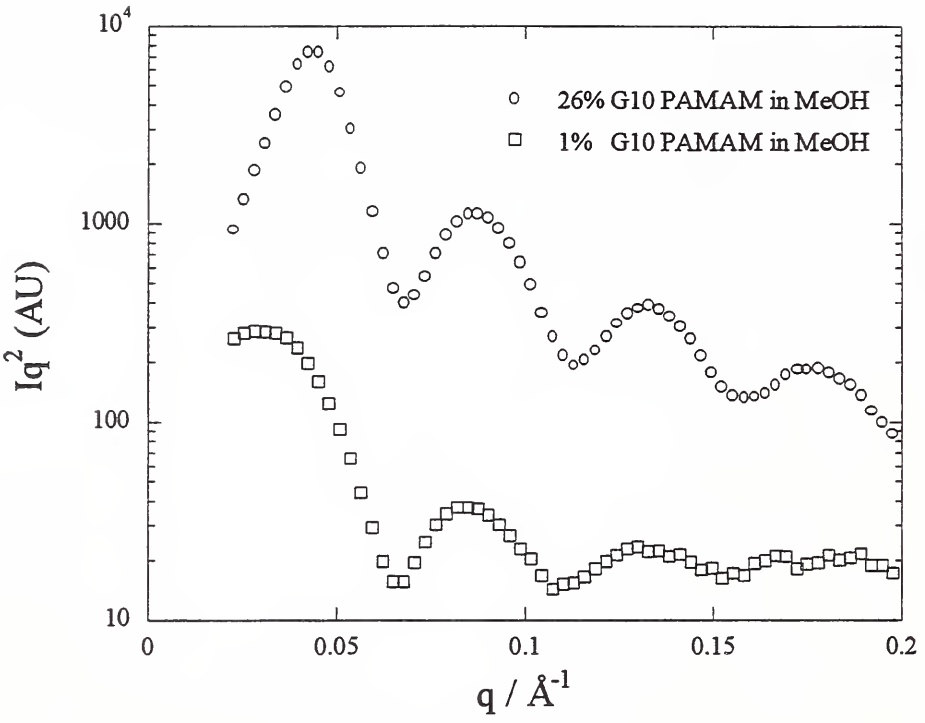

Figure 37. SAXS from PAMAM G10, 1 and 26 %.

TEM Analysis of Dendrimers

NIST: Catheryn L. Jackson, Barry J. Bauer, Eric J. Amis

Outside Collaborators: Henri D. Chanzy, CNRS; Frank P. Booy, NIH; Donald A. Tomalia, MMI

Objectives:

To obtain real space images of dendrimers with resolution to make size measurements using the methods familiar to biological TEM. To determine the smallest size dendrimers that can be reasonably imaged by TEM.

Technical Description:

We have characterized the size, shape and size distribution of PAMAM dendrimer molecules using the technique of positive and negative staining in the TEM. To study the dendrimers in solution using the cryo-TEM method and determine the scope of possible future studies.

Summary:

The PAMAM dendrimers of generation G10 have been successfully imaged by transmission electron microscopy (TEM) using negative staining and cryoelectron microscopy techniques. The sizes of the individual G10 dendrimers are ~14 nm, which is comparable to that measured by light scattering and intrinsic viscosity measurements. Calibration and determination of size distribution is in progress.

For negative staining, better results are obtained if the terminal NH_2 groups on the surface of the dendrimers are charged to NH_3^+ with dilute aqueous HCl. This is a result of better spreading of the stain on the charged dendrimers and less clumping of the dendrimers upon drying the stain. The stains that have been investigated to date include uranyl sulfate, uranyl acetate, sodium silicotungstate, methylamine tungstate (pH=7) and sodium phosphotungstate (pH=7), all in dilute aqueous solution of about 2 %. The best results in terms of negative staining were obtained in methylamine tungstate (Figure 38) and sodium phosphotungstate (Figure 39), which may be because of the neutral pH of these two stains. In the other stains, positive staining of the surface of the dendrimer often was observed, rather than negative staining. In all the stains, the G10 appear spherical and of similar size, within experimental error.

For the cryoelectron microscopy technique, the dilute aqueous solution of G10 is vitrified on a lacey carbon substrate in a very thin film, and image contrast is a result of the difference in density between the dendrimer and the vitrified water or alcohol, and the amount of defocus applied. No staining has been done in conjunction with the cryoelectron microscopy results. This technique has the potential to reflect the state of

the dendrimer in solution, since no drying or staining is done. One variable which cannot be controlled is the concentration of the solution, which might limit the usefulness of this technique to quantitatively study solution properties. Preliminary results on G10 in distilled water, methanol, dilute aqueous HCl and dilute NaCl solution have been obtained. Figure 40 shows the result in distilled water. The size of G10 observed by this method is comparable to the result in negative stain. The shape of the G10 is less uniform than that obtained in negative stain, however, and ordered aggregates of 100-150 nm in diameter are sometimes observed.

Future Plans:

We will determine lower limit of the dendrimer size that can be imaged using negative stain. Preliminary results on G7 and G5 were promising, but a grainy background due to the carbon substrate is one limiting factor. In house improvements in the carbon film used to support the dendrimer are planned (to make a thinner substrate), when our evaporator is functional.

The long term goals include: 1) Determine if aggregation or self-assembly can be further studied by cryoelectron microscopy, or TEM on dendrimer films made by other methods. 2) Apply above techniques to combburst dendrimers being used in blends, to study basic size and shape and eventually blend morphology, as specimens become available from the scattering measurements. 3) Further explore the use of cryoelectron microscopy to study solution behavior, especially after the equipment is obtained in-house.

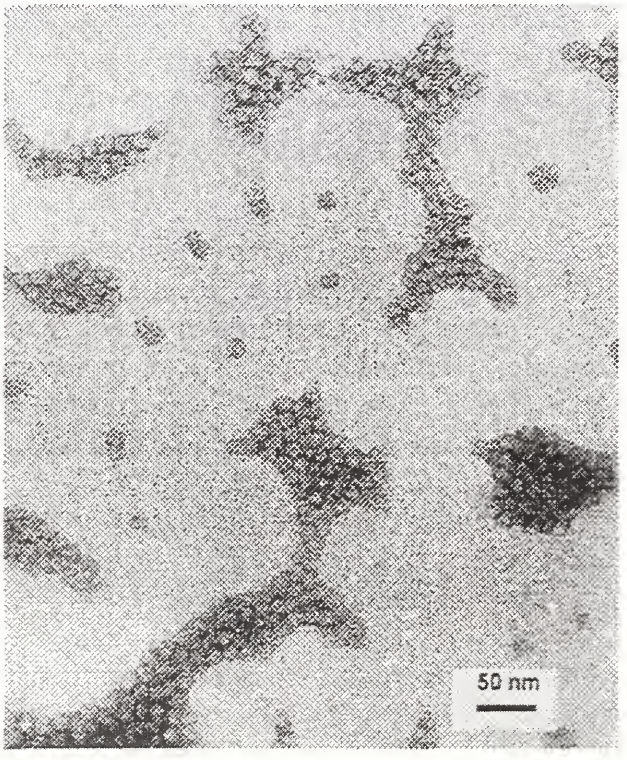

Figure 38. TEM image of negatively stained G10 PAMAM dendrimer (2% methyl amine tungstate).

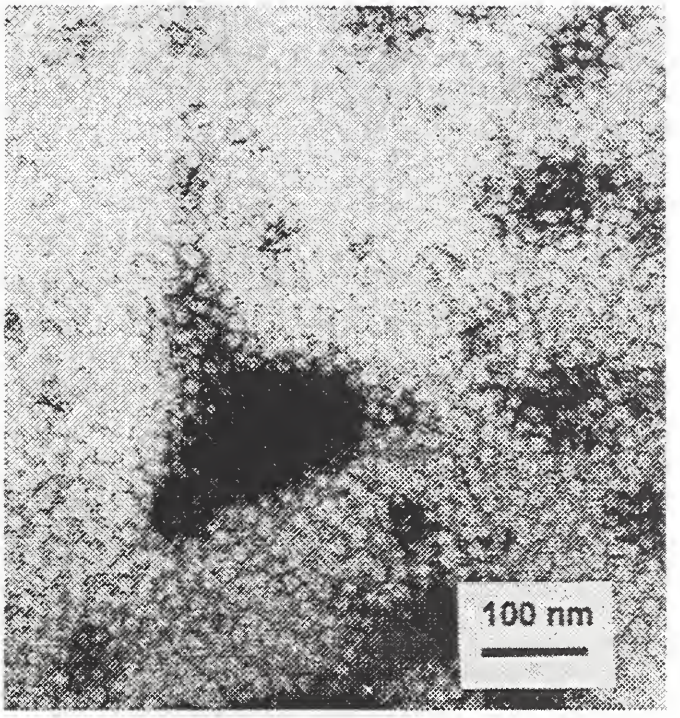

Figure 39. TEM image of negatively stained G10 PAMAM dendrimers (2% sodium phosphotungstate).

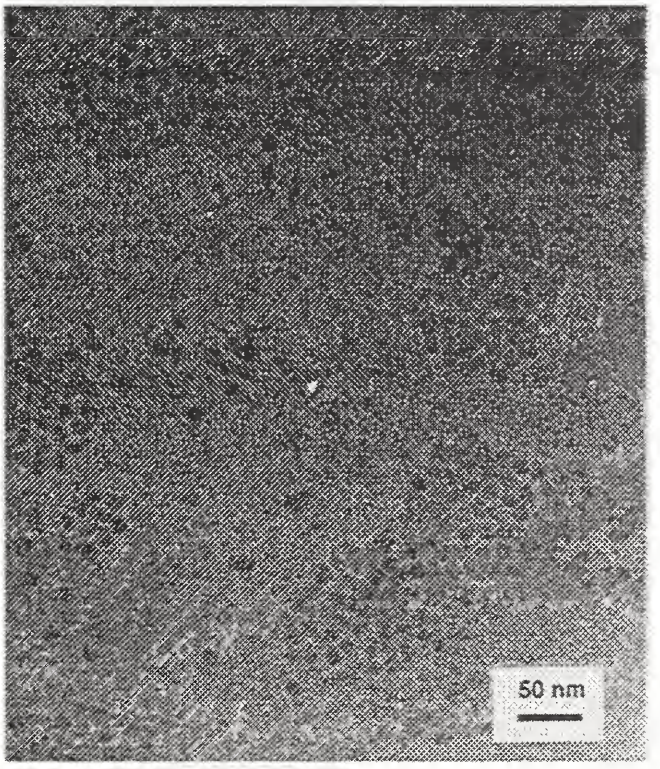

Figure 40. Cryo-TEM image of G10 PAMAM dendrimers in vitrified water.

Dendrimer Monolayer Coatings

NIST: Alamgir Karim, Barry J. Bauer, Dawei Liu, Jack Douglas, Eric J. Amis

Outside Collaborators: Donald Tomalia, MMI; Rolf Scherrenberg, DSM

Objectives:

To see if monolayers of dendrimers can be formed on a surface and how the thickness varies with generation.

Technical Description:

X-ray reflectivity was used to measure the coverage of dendrimers and thickness of monolayers. Atomic force microscopy (AFM) was used to measure the coverage of the dendrimer films.

Summary Report:

Thin film coatings are important for a variety of applications such as protective coatings, dielectric layers, resist layers for lithography, electronic packaging and lubricating surfaces. Contemporary coatings technologies require increasingly thinner films, which in the present day technology consist mostly of polymers, polymer blend materials and more recently self-assembled monolayers. The ability to produce useful and uniform coatings depends on the wettability and adhesion of the film to the substrate. Dewetting of the coatings produces surface roughness and defects that may be detrimental to the performance of the films.

Surfaces may be modified to promote wetting by either chemical (e.g., by HF etching) or by physical (e.g., grafting or self-assembling techniques). Coating dendrimer films provides a novel method for changing the wettability of a substrate. Monolayers of dendrimers coated on a surface offers a versatile and robust means of achieving this goal due to their selective functionality which can be changed in a controllable fashion. Our initial study aims at studying preparation conditions and characterization of properties of dendrimer thin films using X-ray reflectivity (XR) and atomic force microscopy (AFM).

Dendrimer films of different thicknesses were prepared on polished silicon wafers by spin coating from methanol solutions having different dendrimer concentrations. Three generations of dendrimers, 3.5, 4 and 11 were selected for this study. Coatings prepared from the higher concentrations of 1 % and 2 % methanol solutions produced non-uniform films, as measured by AFM and illustrated in figure 41. However, it was possible to prepare uniform films from very dilute methanol solutions for the 3.5 and 4.0 generation dendrimers. Figure 42 shows x-ray reflectivity from ultrathin layers prepared from 0.1 wt% methanol solutions of the three different generations, spun cast at 2000 rpm. The reflectivity is characterized by well defined minimas for G3.5 and G4 films, indicative of smooth films with nominal rms surface roughness (< 10 Å). On the other hand, the minima for the G11 is strongly damped, suggesting a rough surface. From the minima positions, we evaluate the films thicknesses to

be approximately 40 Å, 50 Å and 70 Å respectively for G3.5, G4 and G11. These dimensions are on the order of the size of the dendrimers as determined from other techniques, such as small angle X-ray scattering (SAXS) and small angle neutron scattering (SANS). Thus it appears that the film thicknesses correspond to a monolayer thickness of dendrimers. Further corroboration of these measurements come from the AFM measurements. As shown in figure 43, the surface of the G4 film is quite uniform compared to the G11 which has only a partial layer coverage. The height of the partial layer is ~110 Å, compared to only 70 Å determined by XR due to an averaging of heights in the XR measurements. We anticipate that adjustment of preparation conditions will overcome the partial coverage problem for the higher generations.

Future Plans:

We plan to spin cast dendrigraft layers as well as the type of dendrimer films discussed above and then polymer layers will be spun cast on top of the dendrimer layers and examine the interfacial profile between the polymer and dendrimer by neutron reflection. The dewetting films will be examined by optical microscopy to determine the influence of dendrimer geometry on the type of dewetting patterns formed. We will continue to study dendrimer monolayers, characterizing them as to thickness and uniformity.

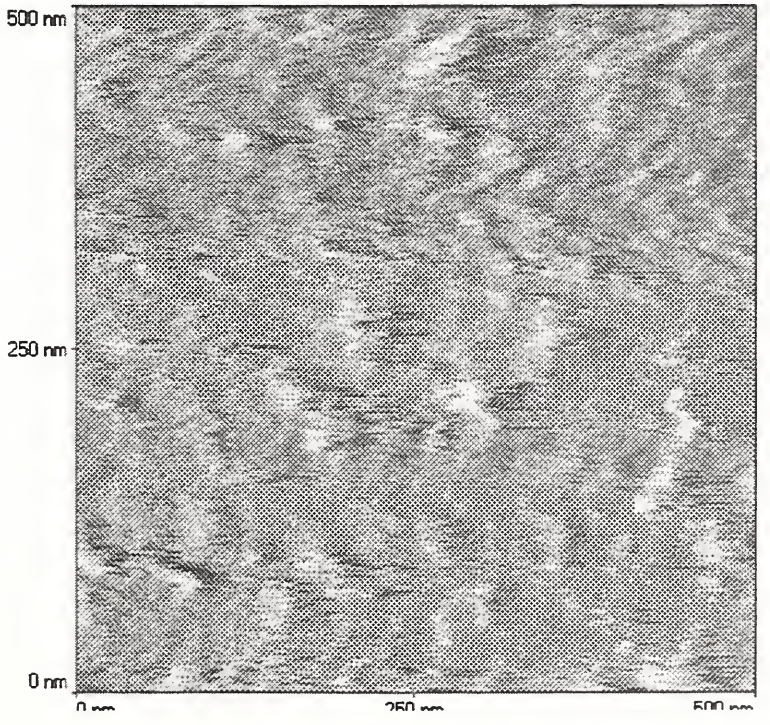

Figure 41. AFM image of a spin coated dendrimer film (G4) on a silicon substrate. The film which is quite uneven, was spun from a 2 % methanol solution at 2000 rpm.

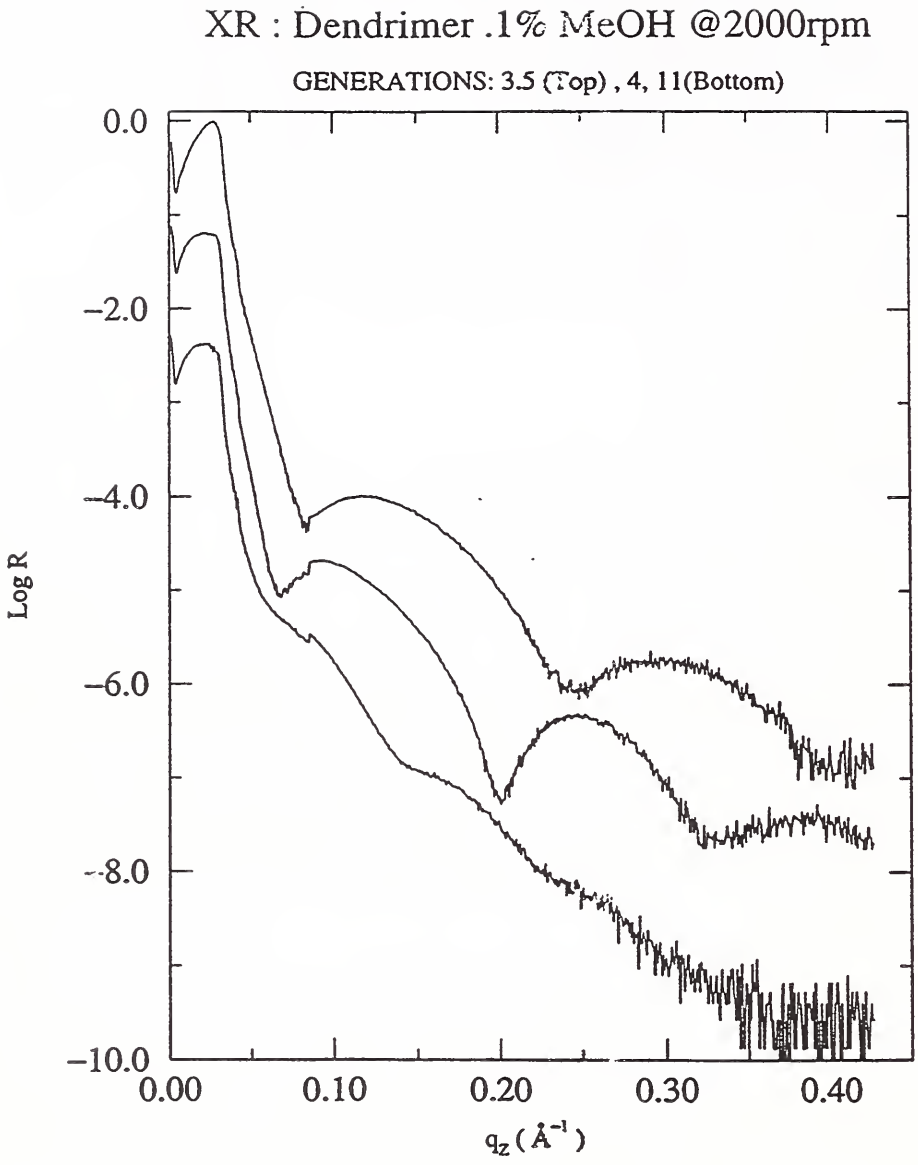

Figure 42. Xray reflectivity results of thin films of PAMAM Generations 3.5, 4, and 11.

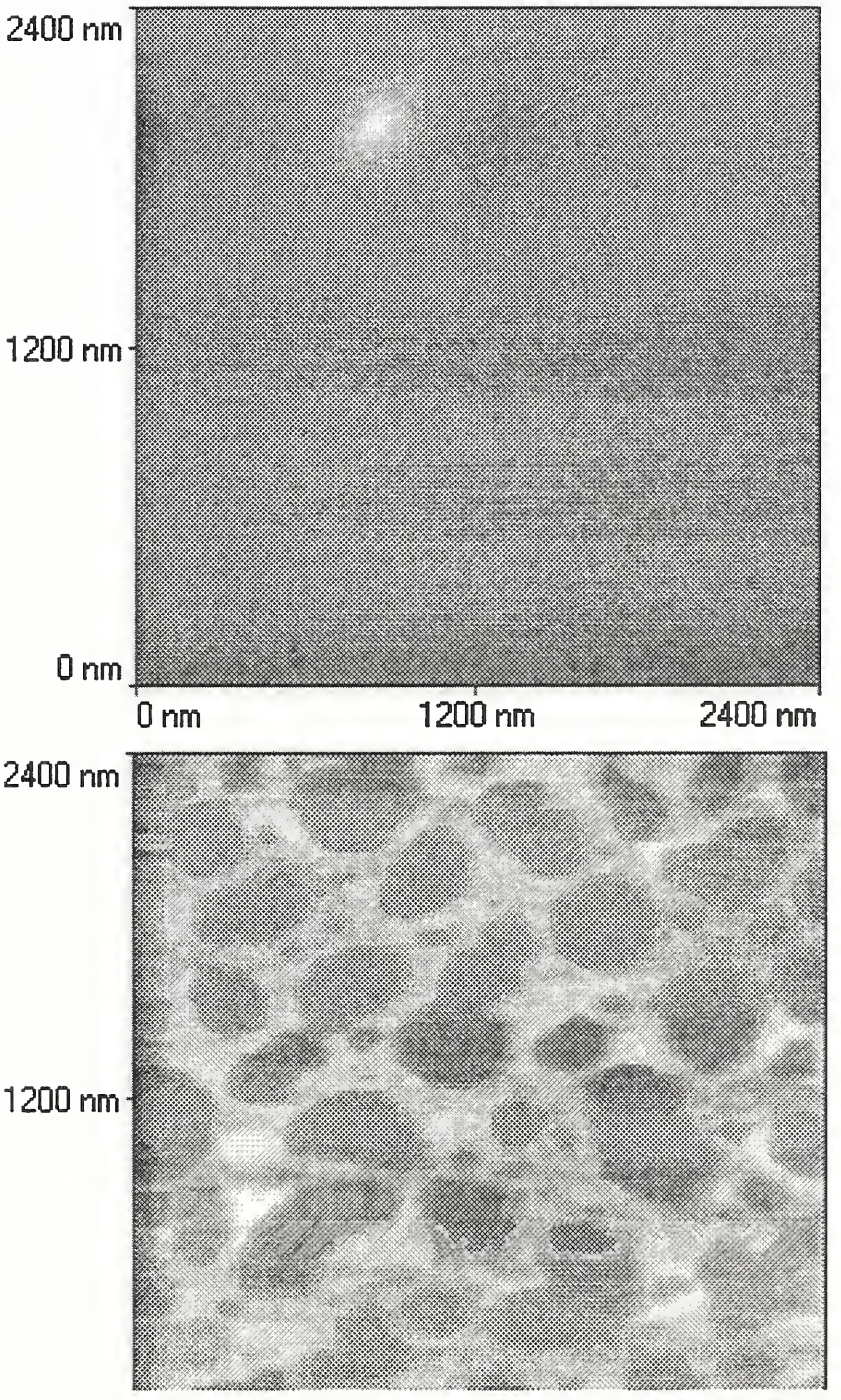

Figure 43. AFM images of a G4 (top) and a G11 (bottom) film spun cast from 0.1 % methanol solution. The bright spot is likely a dust particle.